Application of Electrical Resistance Tomography in Evaluating the Influence of Nozzle Design on the Gas Hold-up in Boiling Bubble Column Reactors

A thesis submitted for the degree of Master of Science in Engineering

Department of Chemical Engineering

University of Cape Town

Harikrishna Sudhakaran

February 2012

Declaration

I am aware that plagiarism is wrong. I declare that this dissertation, submitted for the degree of Master of Science in Engineering at the University of Cape Town, is my own work except where I have explicitly indicated otherwise. It has not been submitted before for any degree or examination at any other university.

Signature of author: .....

Abstract

Bubble column reactors are extensively used in the petro-chemicals industry due to the combined advantages of high rates of heat and mass transfer coupled with low operating and maintenance costs. The complex hydrodynamics brought about by the multiphase nature of such systems offer significant challenges in modelling, analysis and operation, thus making experimental measurement of system response of special importance. One such measurement technique is Electrical Resistance Tomography (ERT).

In this study, the development of an experimental bubble column reactor fitted with 8 rings of 16 electrodes for ERT measurements using an instrument developed at the University of Cape Town (UCT) is described. The initial experiments involving air-water and suspended solid objects served as a calibration and showed the system to be recording the response of the fluid phase reliably. A rigorous experimental programme followed thereafter to evaluate the influence of a particular geometric parameter, namely the aperture angle of the nozzle, on the dispersion of the gas. The comparison on the effect of aperture angles is reported.

The bubble column was then adapted for the investigation of the introduction of gaseous and sub-cooled butane. An experimental program similar to that of the air-water system was then executed and the difference in mixing of both gaseous and sub-cooled systems are compared.

It was found that since the system response to nozzle geometric parameters cannot easily be predicted by theoretical methods, ERT plays a valuable role in assessing the degree of mixing in the given system.

Acknowledgements

I would like to thank my supervisor for providing me with the oportunity to delve into the field of tomography. His insight and advice throughout is appreciated.

Umesh Ramdhani from Sasol for approaching us with this project. His input into the project equates to that of a co-supervisor and for this I am greatly indebted. Also thanks to Sasol Technology (Pty) Ltd their financial support.

Bill Randal and Granville de la Cruz for the installation of the ERT system. Without Bill's expert knowledge into the ERT hardware this project would not have been possible.

Peter Tobias for his highly skilled workmanship in constructing the bubble column.

Lastly but most of all to my parents to whom I thank for their unbelievable support throughout this project.

Contents

List of Figures

List of Tables

Chapter 1

Introduction

1.1 Bubble Column Reactors

Bubble columns are two-phase gas-liquid systems in which a gas is dispersed through a sparger or nozzles and bubbles through a liquid in vertical cylindrical columns (see Figure 1.1). Bubble columns reactors owe their broad application to a number of advantages during operation and maintenance. These are:

- high heat transfer rates
- high mass transfer rates
- reduced wear and tear due to the absence of moving parts
- higher catalyst durability
- ease of operation
- low operating and maintenance costs

Application of bubble colums include absorption, bioreactors and three-phase slurry bubble columns where fine solids are suspended thereby forming a slurry phase. The gas phase contains one or more reactants, while the liquid phase usually contains product and/or reactants (or sometimes inerts).

The investigation of design parameters characterising the operation and transport phenomena of bubble columns have led to better understanding of the hydrodynamic properties, heat and mass transfer mechanisms and the flow regime characteristics that occur during operation. In most columns the gas is fed in at a central point via a sparger or nozzle. As the gas rises this then causes an upward flow of liquid in the centre of the column and a downwards flow of liquid and some bubbles near the walls of the column. The rise velocities of the bubble population in a column significantly affects the hydrodynamics in the column as well as the mass and heat transfer coefficients. For this reason, it is important to obtain all of the properties of the species involved. The average bubble size in a bubble column has been found to be affected by gas velocity, liquid properties, gas distribution, operating pressure and column diameter (Kantari et al. (2005)). The rise velocity of a single gas bubble depends on its size. Thus, the size and rise velocity of a bubble depend on each other and are affected by the same operating conditions.

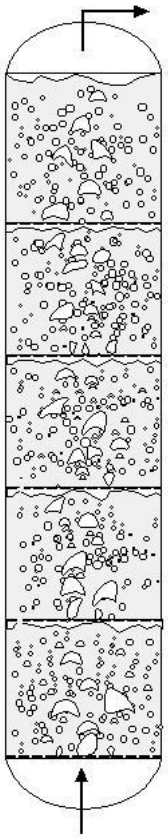

Figure 1.1: Schematic diagram of a bubble column reactor (Shaik and Al-Dahhan (2007))

1.2 Boiling Bubble Column Reactors

In the petrochemical industry, bubble columns are intensively used as multiphase contactors and reactors. A very popular application of bubble columns is in the Fischer-Tropsch (FT) process where the indirect coal liquefaction process is used to produce transportation fuels and other products (Degaleesan et al. (2001)). Many of these reactions in the FT process are exothermic thereby requiring cooling around the bubble column.

Boiling bubble columns are bubble columns, used in the above application, where the latent heat of evaporation of the solvent or feed stream into a reactor is used to remove the heat of reaction within the column. This technique is particularly efficient in systems that are highly exothermic and where heat transfer may be limited due to fouling of internal or external cooling systems. In addition to the cold solvent being used to remove the heat of reaction, the energy released from the flashing solvent also assists in mixing of the bulk liquid (Kim and Lior (1997)).

Due to the flashing effect of the feed stream, local cold spots often develop in and around conventional spargers which may result in ice build up causing nozzle blockage. A significant amount of effort has been invested by SASOL to develop nozzles which limit the extent to which these cold spots become bottlenecks to operation by virtue of introducing the feed stream at different angles thereby producing different mixing patterns. These mixing patterns were found to have removed the development of these cold spots. However the influence of these nozzles on the gas hold-up distribution in a boiling bubble column is not known. As such, the development of new (or the modification of existing) correlations for the degree of mixing or dispersion of the gas phase in such systems would constitute a novel contribution to the field. However, in order to obtain such correlations, a suitable experimental rig together with an appropriate measuring apparatus needs to be constructed and a method to quantitatively determine the effect these nozzles have on the dispersion, needs to be developed.

1.3 Electrical Resistance Tomography

In order to predict and optimise the performance of boiling bubble colmns, models, describing the hydrodynamics within those bubble columns may be developed. The current approach in modelling bubble columns involve the application of computational fluid dynamics (CFD) for predicting the behaviour of a single gas bubble to determine its changes in position and size. This application may then be coupled with a population balance model (PBM) to predict the behaviour of many such bubbles, which are generally distributed in properties such as bubble size, position and rise velocity.

Before such models can be trusted, they must be validated against results obtained from experimental data. With advances in measurement techniques, various imaging and velocimetric techniques have been used to investigate flow regimes in bubble columns. These include:

- high-speed cameras
- Particle Image Velocimetry (PIV)
- Electrical Capacitance Tomography (ECT)
- Electrical Resistance Tomography (ERT)
- Laser Doppler Anemometry (LDA)
- Computer Automated Radioactive Particle Tracking (CARPT)
- γ-ray Computed Tomography (CT)

The process tomography (PT) approach is a technique that has developed rapidly in recent years and which has great developmental potential and wide industrial application prospects for direct analysis of the characteristics of multiphase flows. In tomography the distribution of some physical quantity in an object is determined through the use of any kind of penetrationg wave. Tomographic techniques have been applied to measure the axial and radial gas hold-up distributions in bubble columns. Gamma ray computed tomography has been used for measuring cross-sectional gas hold-up distributions in

bubble columns, gamma-densitometry tomography combined with electrical impedance tomography for measuring gas and solid hold-up distributions in gas liquid solid three phase bubble columns, and multi-modal computed tomography for measuring simultaneously cross-sectional gas and solid hold-up in three-phase bubble columns (Warsito and Fan (2001)). Electrical resistance tomography (ERT) is a type of PT technique and as the name suggests is based on the principle of electrical resistance and is considered to be the most powerful tool among other available tomographic techniques due to its non-radiation, non-invasive, high-speed capability, low construction cost, high safety and suitability for small or large vessels. Moreover, ERT has been successfully used in various industrial investigations for visualisation of concentration profiles and characteristics of the fluid dynamics in gas-liquid two-phase systems (Jin et al. (2007)).

In an ERT system, electrodes are fitted around the periphery of the region to be imaged and an electrical current is injected into that region via. a pair of electrodes. The peripheral voltages resulting from this electrical field are then measured using the remaining electrodes. A detailed explanation of the ERT hardware used in this research is described in Chapter 5. The primary challenge in applying ERT is in using the boundary voltages to reconstruct an image or resistivity map of the measurement region. Chapter 2 will discuss the reconstruction software algorithms used in obtaining these images.

Chapter 2

Literature Review

2.1 Gas Hold-Up in Bubble Columns

The gas hold-up is a dimensionless parameter and arguably the most important variable for characterising the transport phenomena of bubble columns. It is in essence, the volume fraction of gas phase (occupied by the gas bubbles) in the column. All studies on bubble columns examine gas hold-up because it plays an important role in the design and analysis of the columns (Kantari et al. (2005),D.N.Miller (1980),Bukur and Daly (1987),Hikita et al. (1980)).

Of particular importance is that the spatial variations in gas hold-up gives rise to pressure variation, which results in liquid recirculation in the bubble column. This liquid recirculation impacts the rate of mixing, mass and heat transfer. Therefore the ability to predict or measure the gas hold-up profiles in bubble columns makes their design and scale-up more reliable Wu et al. (2001). As a result, this research will only investigate the axial and radial gas hold-up distributions in the bubble column.

Strong liquid circulation in bubble columns is characteristic of the heterogeneous regime of flow where a pronounced radial profile is observed. It is reported by Kantari et al. (2005) that the basic factors affecting gas hold-up are: superficial gas velocity, liquid properties, column dimensions, operating temperature and pressure and gas distributor design. In the subsections below, the findings of various studies on the effects of these

factors are presented.

The gas hold-up gradients and the liquid velocity driven by the gas depends on the superficial gas velocity, column diameter, the nature of the gas-liquid system and the operating conditions, namely the temperature and pressure of the reactor.

2.2 Superficial Gas Velocity

The superficial gas velocity is the average velocity of the gas sparged in the column and is simply expressed as the volumetric flow rate of the gas divided by the cross sectional area of the column. Gas hold-up in bubble columns depends mainly on superficial gas velocity (Shah et al. (1982)). According to Krishna and Maretto (1997); Prakash et al. (2001), for both bubble columns and slurry bubble columns, gas hold-up has been found to increase with increasing superficial gas velocity.

2.3 Gas Sparger

The type and properties of the gas sparger used in a bubble column are important parameters affecting the gas hold-up within the bubble column. According to Bouaifi et al. (2001), the sparger used definitely determines the sizes of the bubbles observed in a bubble column. They also found that the smaller the bubbles the higher the gas hold-up values when using different sizes of orifice gas distributors.

In another study by Luo et al. (1999) the gas hold-up was found to be strongly influenced by the type of gas distribution used. They concluded that the effect was more pronounced especially for gas velocities below 6cm/s. Schumpe and Grund (1986) conducted studies with perforated plate and ring type gas spargers. They concluded that with the ring type distributor the total gas hold-up was smaller and that the small bubble hold-up was smaller. They also added that the contributions of both small and large bubbles at

different superficial gas velocities were lower with ring spargers when compared to the perforated plate.

2.4 Historical overview of ERT

In order to describe in detail the structure and function of an electrical resistance process tomography system, it is necessary to briefly discuss the historical context from which it was derived. Resistivity imaging gained wide acceptance in the 1920s by geophysicists who placed arrays of metallic electrodes into the ground in, for example, Schlumberger and Wenner array configurations (Dickin and Wang (1995)). By injecting current via pairs of electrodes and measuring the resultant voltage response at all other electrodes, a map of the sub-surface strata could be acquired, thereby enabling more precise delineation of, for example, oil-bearing rock. A testament of this technology's simplicity and robustness is that it is still practiced today by many including Qian et al. (2007) and Xie et al. (2010) for mineral exploration.

In the late 1970s, tomographic resistivity measurement techniques using circular arrays of electrodes were popularized by biomedical engineers who regarded them as a low-cost and portable alternative to the increasingly successful x-ray scanner. Since then, clinical ERT systems have undergone continual refinement and now employ multi-frequency spectroscopic methods to detect diseased tissue exhibiting characteristic impedance responses at given frequencies (Bown et al. (1994)).

The conductivity of process liquors can vary considerably from several $\mu S\ cm^{-1}$ (for example, mains tap water) to several hundred $mS\ cm^{-1}$ (for example dissolved soaps). Despite their sophistication, clinical ERT systems are not wholly suited for use in the majority of process applications for two main reasons: due to strict patient safety regulations the instrument cannot supply injected current above an amplitude of 5 mA (peak-peak) at 50 kHz and sub-epidermal tissues are relatively good electrical conductors, usually of the order of $1mS\ cm^{-1}$. Consequently, the clinical ERT systems current sources are not designed to accommodate the wide range of load impedances encountered in many

process applications.

Industrial applications of ERT have been conducted by the groups such as the the pseudo-stationary imaging of gas hold-up in 3-D for typical stirred vessel gas-liquid mixing by Wang et al. (2000), the homogeneous single phase mixing created by different impeller types by Holden et al. (1998) and the application to the semi-batch feed addition of strong brine mimicking the semi-batch addition of a feed reactant by Stanley et al. (2005).

2.5 ERT on Bubble Columns

Electrical resistance tomography or ERT is an imaging technique that can be used to determine the internal structure of an object or vessel non-intrusively as shown by Fransolet et al. (2001). Electrodes are placed around the periphery of the region to be imaged and an electrical field is generated in that region. This current injection is done by driving a sinosodial current between two of the electrodes. The peripheral voltages resulting from the electrical field are measured using the remaining electrodes. By repeating this process, selecting successive adjacent electrode pairs to drive current through, a data frame is built up that can be used to reconstruct an image or resistivity map of the measurement region.

2.5.1 Reconstruction Algorithm

The voltage measurements obtained from the ERT instrument needs to be used in order to obtain the conductivity distribution over the electrode plane, which can then be translated to a voidage plane using Maxwell's equation (see Eq. 2.15). The reconstruction algorithms used in this research for the offline reconstruction are based on that developed by Long (2006).

2.5.2 The Forward Problem

The Forward Problem involves predicting the boundary potentials in a medium from a known conductivity distribution. In order to do so, a governing equation that describes the current flow in a medium needs to be developed. This governing equation is called Poisson's Equation and its derivation is described below.

As described by Herholtz (2003) and Fransolet et al. (2002) the current density in a conductive medium is subject to an electric field by the following relationship:

$$J = \sigma E \tag{2.1}$$

and the electric field is related to the electric potential, by

$$E = -\nabla \cdot \nu \tag{2.2}$$

where: J is the current density in (A/m^2)
σ is the conductivity in (S/m)
E is the electric field in (V/m)
ν is the electric potential in V

However if the conductive medium is not a current source, such as that in the bubble column reactor, then all the current entering a point must also leave that same point. Therefore:

$$\nabla \cdot J = 0 \tag{2.3}$$

Substituting equations 2.3 and 2.2 into equation 2.1 yields Poisson's equation in vector form:

$$\nabla \cdot (\sigma \nabla \nu) = 0 \tag{2.4}$$

or in the two-dimensional case:

$$\frac{\partial}{\partial x}\left(\sigma\left(x,y\right)\frac{\partial V\left(x,y\right)}{\partial x}\right) + \frac{\partial}{\partial y}\left(\sigma\left(x,y\right)\frac{\partial V\left(x,y\right)}{\partial y}\right) = 0 \tag{2.5}$$

with the following boundary conditions:

$$\int_{\Gamma_1} \sigma \frac{\partial \nu}{\partial n}\, ds = I \tag{2.6a}$$

$$\int_{\Gamma_2} \sigma \frac{\partial \nu}{\partial n}\, ds = -I \tag{2.6b}$$

$$\nu|_{\Gamma_3} = \text{unknown constants} \tag{2.6c}$$

$$\frac{\partial \nu}{\partial n}|_{\Gamma_4} = 0 \tag{2.6d}$$

where: Γ_1 is the source electrode surfaces

Γ_2 is the sink electrode surfaces

Γ_3 the set of other electrode surfaces

Γ_4 the set of insulated surfaces of the sensor

The Forward Problem involves solving equation 2.4 by guessing σ (the internal conductivity distribution) and then solving for the electric potential across the region. An analytical solution to equation 2.4 does not exist in general, therefore a numerical solution is necessary. Therefore a numerical method is needed to achieve this. The finite difference method (FDM) and the finite element method (FEM) are two such numerical tools that can be applied. Whilst the FDM is easier to apply, the accuracy of the solution obtained using this method is poor in multi-dimensional cases or where the boundary is irregular in shape. The FEM, which is designed for multi-dimensional domain, is the preferred method for solving the Forward Problem. A detailed description of the FEM is beyond the scope of this thesis; an interested reader is referred to Herholtz (2003), Fish and Belytschko (2007) and Burnett (1987).

2.5.3 The Inverse Problem

The main objective when using ERT is to find the conductivity distribution in the region to be imaged. Solving for Equation 2.4 for conductivity, given the boundary voltages and

currents is called the inverse problem. Since an accurate solution for the conductivity distribution cannot be achieved analytically, the forward problem is solved iteratively, by changing the conductivy distribution , σ, using methods described by Hua and Woo (1990), until the boundary voltages are close enough to the measured voltages. According to Dickin and Wang (1995), the Newton-Raphson algorithm was shown to produce the best results of such inverse methods. As a result, the Newton-Raphson algorithm was chosen in this research to solve the inverse method.

Newton-Raphson Algorithm

In principle, the Newton Raphson method can be compared to Newton's method in 1-D where an initial guess is made, then a tangent is taken at that point and our new guess for the answer is updated where the tangent cuts the x-axis. This is then repeated for the updated guess, until the answer converges close to the true solution. When applying the Newton-Raphson algorithm in the context of the multi-dimensional inverse problem, the quantitative reconstruction process is initiated when a set of resistivities for each element is fed into the forward problem solver. In order to reduce the number of iterations performed by the algorithm to reach a final solution, it is imperative to ensure that the initial set of resistivities is relatively close to the final set. The forward problem is then solved using the FEM-based solver and the resultant set of calculated boundary voltages are then compared to those from the data acquisition system. The the mean square error between measured and computed values for the boundary voltages is calculated by using Equation 2.7.

$$E(\sigma) = \frac{1}{2}\left[f(\sigma) - V_0\right]^2 \tag{2.7}$$

where $f(\sigma)$ is the forward operator that computes the boundary voltages given a conductivity distribution (σ) and V_0 is the actual voltage measurements.

The idea is to minimise the error function, $E(\sigma)$ such that it is less than a pre-determined value. If not, the resistivity of each element is updated via the NewtonRaphson technique and then fed into the forward solver for another iteration. To do this, $E(\sigma)$ is differentiated with respect to σ and then equated to zero, to result in:

$$E'(\sigma) = [f'(\sigma)]^T (f(\sigma) - V_0) = 0 \tag{2.8}$$

where $[f'(\sigma)]_{i,j} = \frac{\partial f_i}{\partial \sigma_j}$ is called the Jacobian matrix and will hence be referred to as J.

Next, perform a Taylor series expansion of $E'(\sigma)$ around σ_0 and taking the linear terms to get what is called the called the Hessian matrix:

$$E'(\sigma) = E'(\sigma_0) + E"(\sigma_0)\,\Delta\sigma \tag{2.9}$$

where:

$$E"(\sigma_0) = J^T \cdot J + [J'][J - V_0] \otimes J^T J \tag{2.10}$$

and $\otimes$ is the Kronecker matrix product. Since J' is difficult to calculate and relatively small, the second term in Eq.2.10 is usually omitted. Therefore the Hessian matrix is modified to:

$$E"(\sigma_0) = J^T \cdot J \tag{2.11}$$

Substituting equations 2.8 and 2.11 into equation 2.9 results in:

$$\Delta\sigma = \left[J^T \cdot J\right]^{-1} J^T [f(\sigma_0) - V_0] \tag{2.12}$$

The error, $E(\sigma)$, is therefore reduced after updating σ_0 by adding it to $\Delta\sigma$. This process can be applied iteratively until some tolerance criterion is met. The Newton-Raphson algorithm illustrated in Figure 2.1

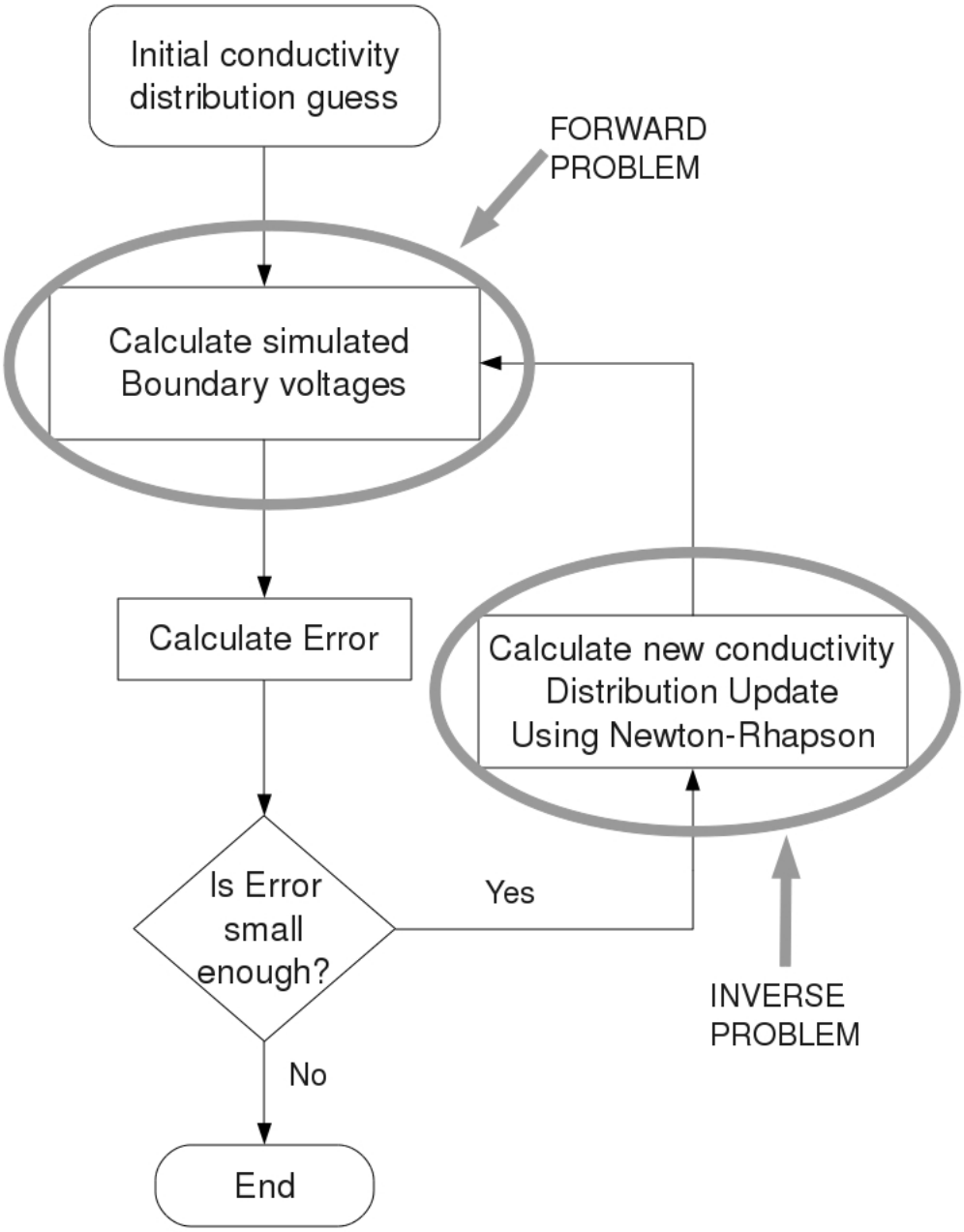

Figure 2.1: The Newton-Raphson algorithm

Ill-conditioning and Regularisation

The inverse problem in ERT according to Herholtz (2003), by nature is ill-conditioned, meaning that large changes in the conductivity distribution causes small changes in the

voltage distribution. Some form of regularisation approach, where the inverse method is stabilised, is therefore required. This is achieved by modifying the error function, equation 2.7, to include a small constant that penalises rapidly changing resistivities, which means that the effect of small data errors will be reduced. The new error function will now be in the form shown in Equation 2.13.

$$E(\sigma) = \frac{1}{2}\left[f(\sigma) - V_0\right]^2 + \lambda Q(\sigma) \tag{2.13}$$

where $Q(\sigma)$ is the regularisation operator and λ is known as the regularisation parameter that determines the degree of regularisation. As λ increases, the greater the regularisation or smoothing. The conductivity update function then becomes:

$$\Delta\sigma = \left[J^T \cdot J + \lambda Q(\sigma)\right]^{-1} J^T \left[f(\sigma_0) - V_0\right] \tag{2.14}$$

which is an example of Tikhonov regularisation, and Pinheiro et al Pinheiro et al. (1997) have suggested many different regularisation operators to calculate $Q(\sigma)$.

Equation 2.14 is implemented recursively implemented until the error (Equation 2.13) reaches below an acceptable value. The validation of the ERT system and the reconstruction algorithm is validated in the next chapter.

2.6 Estimation of Gas Hold-Up Profile in a Bubble Column using ERT

With the conductivity data from the ERT instrument, the local gas volume fraction (ε_g) can be determined by applying the Maxwell equation (see Eq. 2.15):

$$\varepsilon_g = \frac{2\sigma_1 + \sigma_2 - 2\sigma_{mc} - \frac{\sigma_{mc}\sigma_2}{\sigma_1}}{\sigma_{mc} - \frac{\sigma_2}{\sigma_1} + 2(\sigma_1 + \sigma_2)} \tag{2.15}$$

where:

σ_1 is the conductivity of the first phase in Sm^{-1}

σ_2 is the conductivity of the second phase Sm^{-1}

σ_{1mc} is the local value of the mixing conductivity distribution Sm^{-1}

If the second phase is assumed to be a non-conductive material, such as air or butane in this study, the above equation can be simplified as follows:

$$\varepsilon_g = \frac{2\sigma_1 - 2\sigma_{mc}}{2\sigma_1 + \sigma_{mc}} \tag{2.16}$$

the local (mesh) mixture conductivity ,σ_{mc}, is conductivity distribution from the ERT reconstruction.

2.7 Effect of Superficial Gas Velocity on the Gas Hold-Up from Experiments Using ERT

Images of the gas hold-up shown by experiments conducted by (Fransolet et al. (2001)) indicate that there is a clear increase of the average gas hold up when increasing the gas velocity as discussed in Section 2.2. The data corresponds to scans at one fixed axial location that is well away from entrance or free surface effects. Average gas hold-up can be calculated by averaging pixel values (weighted with respect to pixel area fraction) over the entire cross-section. Fransolet et al. (2001) has shown that the changing of these averaged hold-up data versus the superficial gas velocity also indicates that the gas hold-up increases with the superficial gas velocity. The homogeneous regime is characterised by the linearity of the gas hold-up versus gas velocity at lower gas velocities, and the fully developed heterogeneous regime is observed at higher gas velocities (Fransolet et al. (2001)). More significantly Fransolet et al. (2001) obtained the radial gas hold-up distribution at different superficial gas velocities using both ERT and optical probes, see Figure 2.2. The radial gas hold-up profiles determined using ERT is achieved by using Eq. 2.16. It can be seen that the gas hold-up values obtained using ERT correlate favourably with those from the optical probes. An equation to model these radial profiles was then attempted by Fransolet et al. (2005). This modelling of the radial profiles is described in the following section.

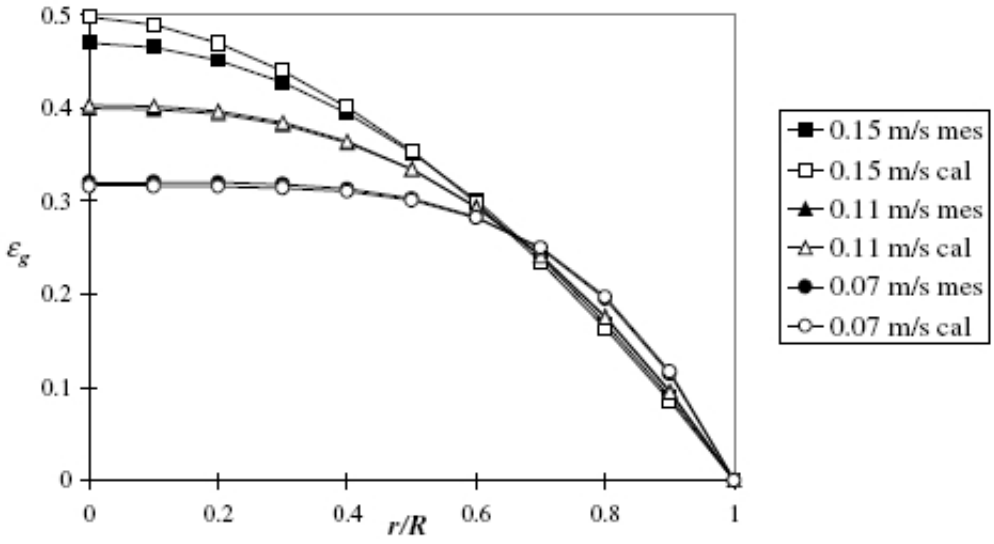

Figure 2.2: Gas hold-up profiles predicted using ERT ('cal') compared with those measured with the optical probe ('mes') by Fransolet et al. (2001)

2.8 Quantification of the Degree of Gas Dispersion from the Radial Gas Hold-Up Profiles

Over the past thirty years, a number of experimental measurements of gas hold-up and gas hold-up profiles in bubble columns have been reported in literature. The high level complexity of the system makes it difficult to apply fundamental models to predict the radial gas hold-up profile for all types of columns. According to Nassos and Bankoff (1967) the following equation for the radial hold-up profile is proposed:

$$\varepsilon_G = \widetilde{\varepsilon}_G \left(\frac{n+2}{n} \right) \left[1 - \left(\frac{r}{R} \right)^n \right] \tag{2.17}$$

where:

$\widetilde{\varepsilon}_G$ is the cross-sectional mean gas hold-up

n is an exponent parameter

$\frac{r}{R}$ is the dimensionless radial position

Equation 2.17 is a power law that is of parabolic nature. The value of n is indicative of the steepness of the hold-up profile. When n is large the profile is flat and when it is small the profile is steep. Equation (2.17) has been modified over the years and in 1991, Luo and Svendsen (1991) modified it to:

$$\varepsilon_G = \tilde{\varepsilon}_G \left(\frac{n+2}{n+2-2c} \right) [1 - c \left(\frac{r}{R} \right)^n] \tag{2.18}$$

where c allows the possibility of non-zero gas hold-up close to the wall.

Applying Eq. (2.18) to the gas hold-up data from experiments conducted by Joshi et al. (1998), n was found to vary from 1.4 to 11 and c varied from 0.5 to 1. Since a theoretical prediction for gas hold-up profile is non-existent, correlations are needed to evaluate n and c based on the general operating variables and physical properties of the system in order to estimate the gas hold-up profile by Eq. (2.18). Based on experimental observations and dimensional analysis conducted by Wu et al. (2001), the following functional dependence was proposed for parameters n and c:

$$n = af\left(Re_G, Mo_L, Fr_G\right), \qquad c = \beta\zeta\left(Re_G\right)$$

where:

$$Re_G = \frac{DU_{Sg}\left(\rho_L - \rho_G\right)}{\mu_L}, \qquad Mo_L = \frac{U_{Sg}^2}{gD}, \qquad Fr_G = \frac{g\mu_L^4}{\left(\rho_L - \rho_G\right)\sigma_L^3}$$

and

$$n = 2.188 \times 10^3 Re_G^{-0.598} Fr_g^{0.146} Mo_L^{-0.004} \tag{2.19}$$

$$c = 4.32 \times 10^{-2} Re_G^{0.2492} \tag{2.20}$$

The main problem with Equation 2.18 is that it inhibits its application to radial hold-up profiles that are not parabolic in nature. Therefore a different method needs to be developed to analyse the dispersion of the gas-phase from all types of radial gas hold-up profiles. This method that has been developed during the course of this research and is

discussed in Chapter 7.

Chapter 3

Thesis Objectives

The primary interest in this work is to quantitatively assess the influence that nozzle aperture angles have on the radial distribution of the population of gas bubbles in a bubble column and therefore ascertain the optimum aperture angle in terms of maximising the degree of mixing within the column. As described in the Introduction, one of the main approaches to achieving this, is to simulate the flow of gas bubble in a bubble column using CFD. However chapter 2 has shown that ERT can be applied non-intrusively to directly measure the gas distribution inside a bubble column.

Apart from the application of tomography in analysing conventional bubble columns, another important investigation in this study is the effect of the flashing of sub-cooled liquid butane, on the mixing in the column. It is anticipated that the agitation and hence degree of mixing within the system will increase due to the flashing effect and should be captured by the tomographic measurements..

Section 2.8 has shown that the current method of evaluating the degree of mixing of the gas phase in a bubble column cannot be applied to all systems. Therefore an important objective of this study is to develop a method in which to quantify the degree of dispersion for all types of systems.

In order to understand the effect of different aperture angle has on the dispersion of the gas, a simple model describing the flow of a bubbles rising in a bubble column is used.

This model will be used with different initial distributions of bubble size (which is equivalent to different inlet distributions caused by different nozzle designs) to determine the significance of this on the hydrodynamics. The point is to demonstrate that in a very simple flow pattern, the inlet distribution strongly influences the gas distribution inside the reactor. If there is no influence under such a simple set of hydrodynamics, then there will be an even weaker dependence as the flow becomes more turbulent. This is therefore a necessary first step even before constructing any equipment.

Chapter 4

Development of A Simple Bubble Column Reactor Model

A simplified model is developed to establish whether different initial bubble size distributions will have a significant effect on the overall gas hold-up in the column. The development of this model has no direct impact on the final results obtained in this thesis but is necessary in order to justify an experimental investigation into the effect each nozzle has on the radial gas hold-up distribution in the column.

4.1 Conditions for a Simple Bubble Column Model

The model is simplified using the following assumptions:

- The bubbles rise in a stagnant fluid, meaning the changes in the liquid velocity distributions has been ignored. This would mean that the bubble will move in a straight line in the vertical direction. This would be the case when one bubble rises in the column..
- Bubble coalescence and break-up were ignored.
- Expansion of a bubble due to the decrease in pressure as the bubble moves up was ignored, as it is inconsequential for such a small rise distance.

- Deformation of a bubble was ignored, i.e. the bubbles stays spherical.
- There are no internal circulations within the bubble and no slip exists between the boundary.
- In performing the force balance on a bubble, the two main forces (buoyancy and drag) were used. The minor forces according to Magnaudet and Eames (2000), the added mass force, the inertial force and the shear lift force can be ignored due to velocity gradients at the wall of the column being low.

4.2 Bubble Rise Velocity Formulation - Force balance

The rise velocity (usually called the terminal rise velocity in stagnant liquids or slip velocity in the case of moving liquids) of bubbles in liquid dispersions is the main factor that decides the gas phase residence time and hence the gas hold-up in a bubble column. The rise velocity of a bubble is calculated by performing a force balance on it. As mentioned above, these forces are the bouyancy and the drag force. The force balance, therefore is:

$$V_b\,\rho_b\,\frac{\partial \mathbf{v}}{\partial t} = \underbrace{(\rho_l - \rho_b)\,V_b\,g}_{\substack{\text{Bouyancy}\\ \text{Force}}} + \underbrace{\frac{1}{2}\,C_D\,\pi\,R_b^2\,\mathbf{v}^2}_{\substack{\text{Drag}\\ \text{Force}}} \tag{4.1}$$

where - $\mathbf{V_b}$ is the volume of the bubble
- $\mathbf{C_D}$ is the drag coefficient
- $\mathbf{R_b}$ is the radius of the bubble

The drag coefficient, C_D , is the proportionality constant found in the drag force term in Equation 4.4. This coefficient varies depending on the physiochemical properties of the liquid and the Reynolds number, Re. Reynolds number is a dimensionless incorporates size, velocity and kinematic viscosity of the object. It is known that Re has the biggest effect on C_D and as Re increases, C_D will decrease. Since the values of Re in this model

were found to be extremely high (in the order of 10^3), a drag coffecient of 0.95, proposed by Karamanev and Nikolov (1992) is used for Re greater than 135. This value of C_D was representative of bubble rise times observed during the experiments, which is shown in the next section.

4.3 Simulation Conditions for the Column

The conditions used in the simulations are the ones used experimentally in this study.

- A water level height of 1.6m, was used which represents that used in the pre-liminary air-water experiments.
- An initial bubble velocity of $0m.s^{-1}$ was applied to the bubbles.

4.4 Rise of a Single Bubble

Using Eq. the movement of a single bubble was tracked to determine whether its residence time is reflective of that observed during the preliminary experiments conducted identical to ones in Chapter 5. The initial size of bubbles observed experimentally were between 1mm and 5mm. As a result these two values were chosen for the simulations for initial bubble size. The results obtained for these two bubbles is illustrated in Figure 4.1.

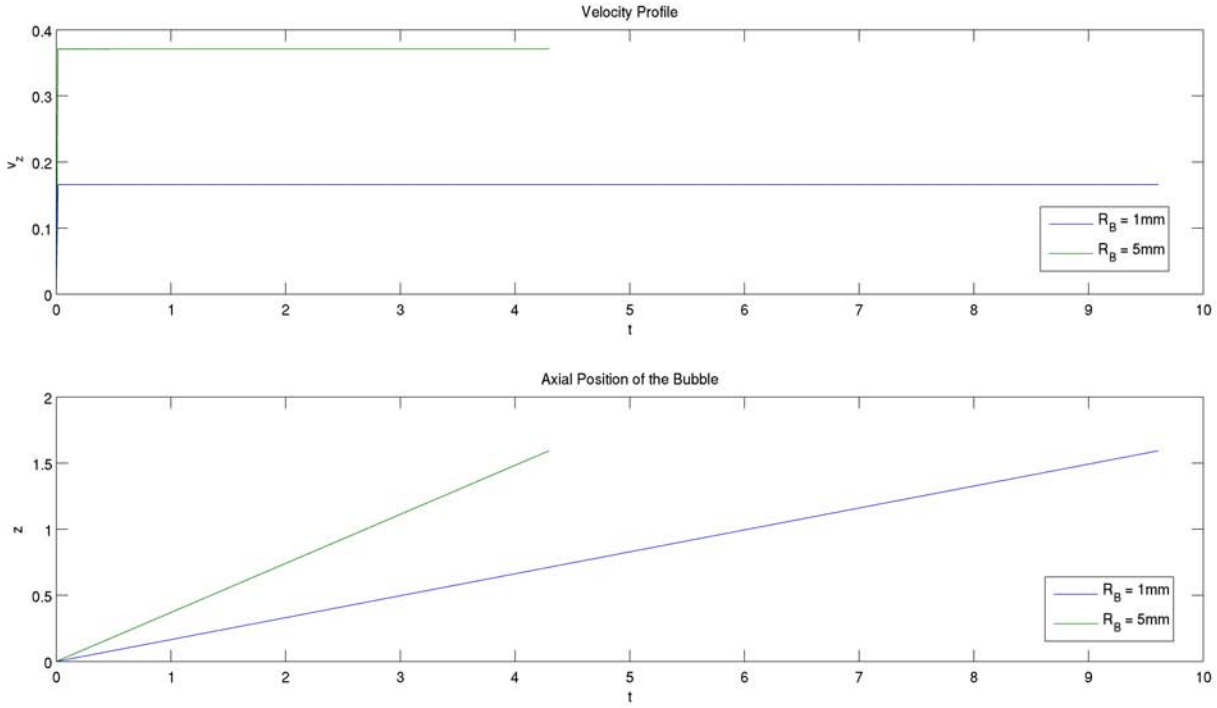

Figure 4.1: Velocity Profile and Axial Position of the Single Bubbles

Figure 4.1 shows the residence time (time it takes for the bubble to move from the bottom to the top of the column) for the 1mm and 5mm bubbles to be 9.6s and 4.3s respectivley. This follows the physical principle that bigger bubbles rise faster than smaller ones. The order of magnitude of the residence times also falls within that observed during the experiments. It can also be seen from Figure 4.2 that the terminal velocity (16.6cm/s and 37.1cm/s for the 1mm and 5mm bubbles, respectively) is reached in a short time, which is to be expected of very small bubbles. These rise velocities are reflective of that shown by Clift (1978).

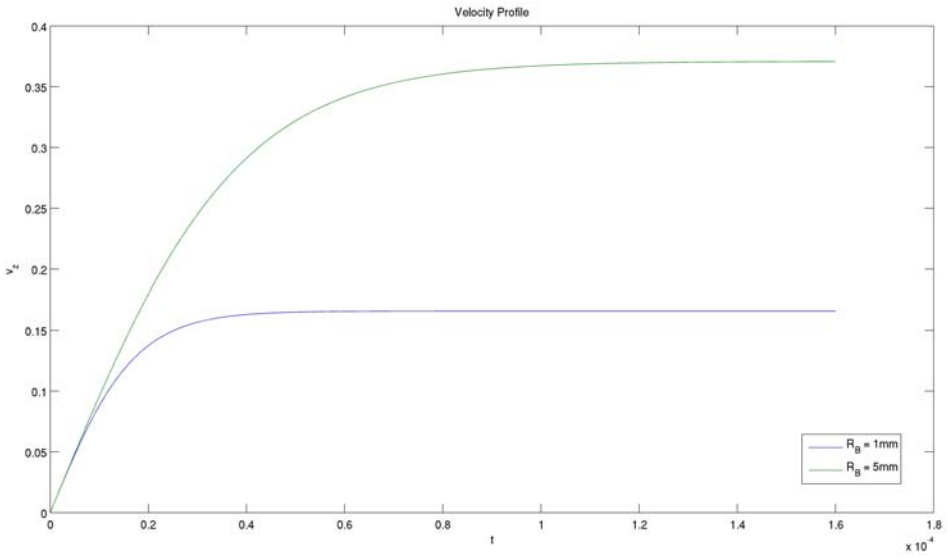

Figure 4.2: Time Taken to Reach the Terminal Rise Velocities Using the Bubbel Rise Simulation

4.5 Effect of Different Bubble Size Distributions on the Overall Gas Hold-Up

The initial bubble size range was chosen between the two sizes, 1mm and 5mm, used for the single bubble simulations as this range fell within the bubble sizes observed in the column during the preliminary experiments. This range was divided into 20 bubble size classes. Three bubble size distributions were chosen; normal, uniform and exponential to represent a varied initial bubble size population. The rise velocities for each bubble class was calculated and the time it takes each bubble in a size class to reach the top of the column (residence time) was calculated. Since we have the distribution of the flow into each bubble class, we can then calculate the number of bubbles formed per second in each bubble size class. This is then multiplied by the residence time to give the hold-up of each bubble class column. Once all the hold-ups of each class is calculated, the total hold up can be determined. The results for each distribution is shown in the following sections.

4.5.1 Normal Distribution of Bubble Size

Figure 4.5.1 show the distribution of the volumetric flow rate into each bubble size class. The overall gas hold up obtained is 1.24%.

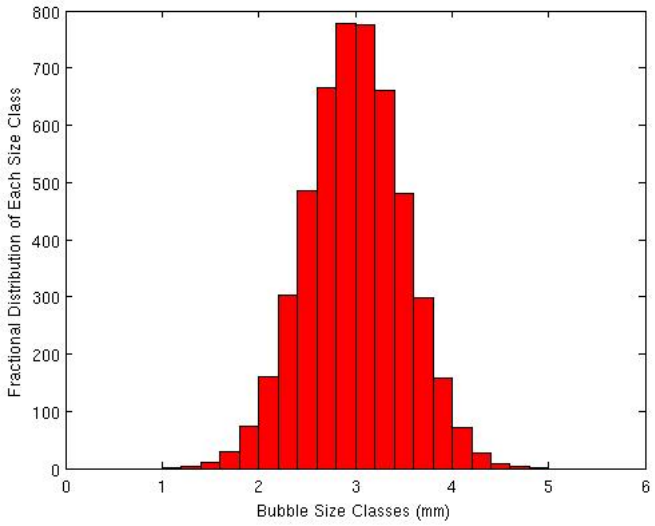

Figure 4.3: Normal Distribution of the Volumetric Flow rate into each Bubble Classes

4.5.2 Uniform Distribution of Bubble Size

Figure 4.5.2 show the distribution of the volumetric flow rate into each bubble size class. The overall gas hold up obtained is 1.31%.

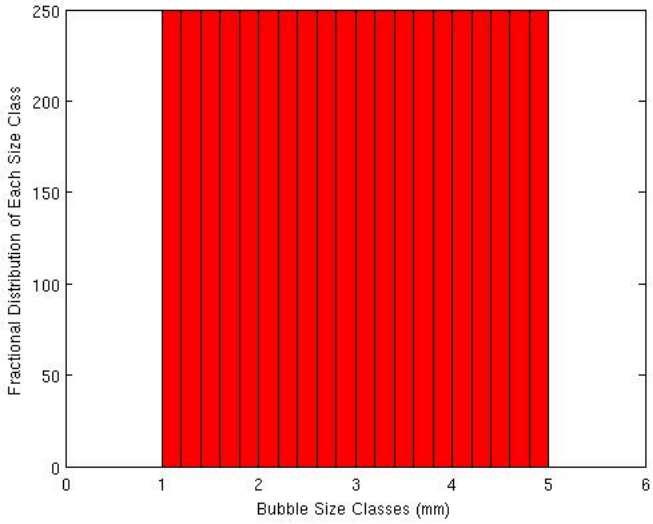

Figure 4.4: Uniform Distribution of the Volumetric Flow rate into each Bubble Classes

4.5.3 Exponential Distribution of Bubble Size

Figure 4.5.3 show the distribution of the volumetric flow rate into each bubble size class. The overall gas hold up obtained is 1.84%.

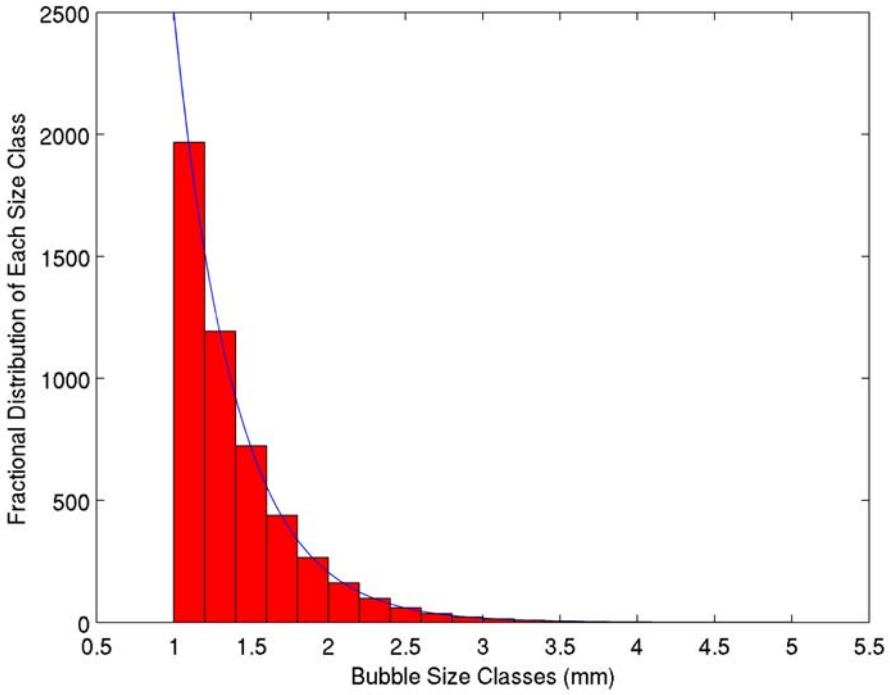

Figure 4.5: Exponential Distribution of the Volumetric Flow rate into each Bubble Classes

Despite the simplified assumptions made in these models, the differences in the gas hold-up for varied inlet bubble size distributions are large enough to suggest that gas hold-up is clearly influenced by the inlet bubble size distribution. This then justifies further investigation in determining the effect off different nozzle designs on gas hold-up using experimental methods.

Chapter 5

Experimental Materials and Methods

In this chapter an experimental system that can satify the thesis objetives of both identifying the optimum nozzle aperture angle as well as the effect of the flashing butane has on the degree of mixing is described. Gaseous synthetic air will be used to determine the effect of different nozzle aperture angles on the degree of mixing. Gaseous and sub-cooled liquid butane will be used to determine the effect of flashing on the degree of mixing. Butane is used as it is a hydrocarbon used in the petrochemical industry with a relatively high boiling temperature (-0.5^oC at atmospheric pressure), which is manageable in a lab-scale experiment.

5.1 Process Flow Diagram

Before any design or construction can take place a process flow diagram of the system needs to be drawn. Figure 5.1 shows the process flow diagram for the air and butane experiments conducted in this study.

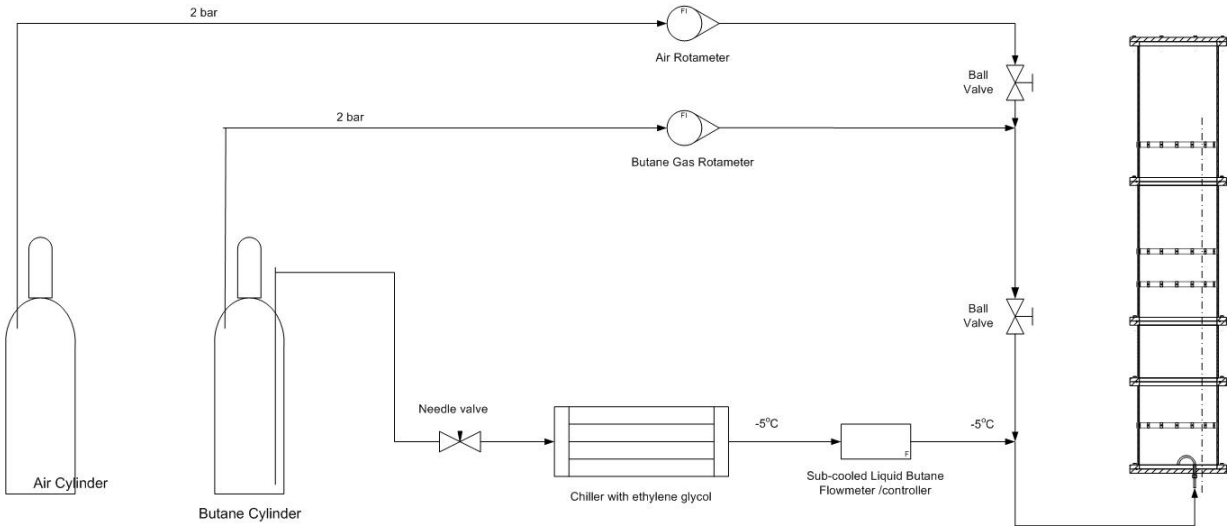

Figure 5.1: Process Flow Diagram of the Butane Experiments

The whole experimental rig is housed in a glass covered chamber with a gas extraction system to remove the potentially dangerous butane gas, from any possible ignition source, to the atmosphere. The flow of the air and gaseous butane is controlled by individually calibrated rotameters. The flow of liquid butane is measured with a Coriolis meter. The Coriolis instrument is also able measure the temperature and density of the fluid moving through it, which will aid in determining if the sub-cooled butane is flowing through to the bubble column at the right temperature. The flow of liquid butane is effectively controlled manually with the use of a needle valve.

5.2 The Bubble Column

The bubble column used in this research was designed to provide a scaled-down version of that used in the petro-chemical industry. The same height to diameter ratio as that used in industry was applied in the design. As a result, a column with an inner diameter of 290mm with a wall thickness of 5mm and a height of 1660mm was designed. This is shown in the Figure 5.2. The material used to construct the column is perspex, with a stainless steel section fitted at the bottom. Perspex was chosen owing to its colourless and non-conductive properties. The stainless steel section has a heating band around it, which in turn is connected to a temperature control system. This is necessary to maintain

the temperature of the water in the column during the operation of the flashing butane as the continuous flashing will cause a decrease in temperature that will eventually lead to the nozzle being blocked due to ice build up.

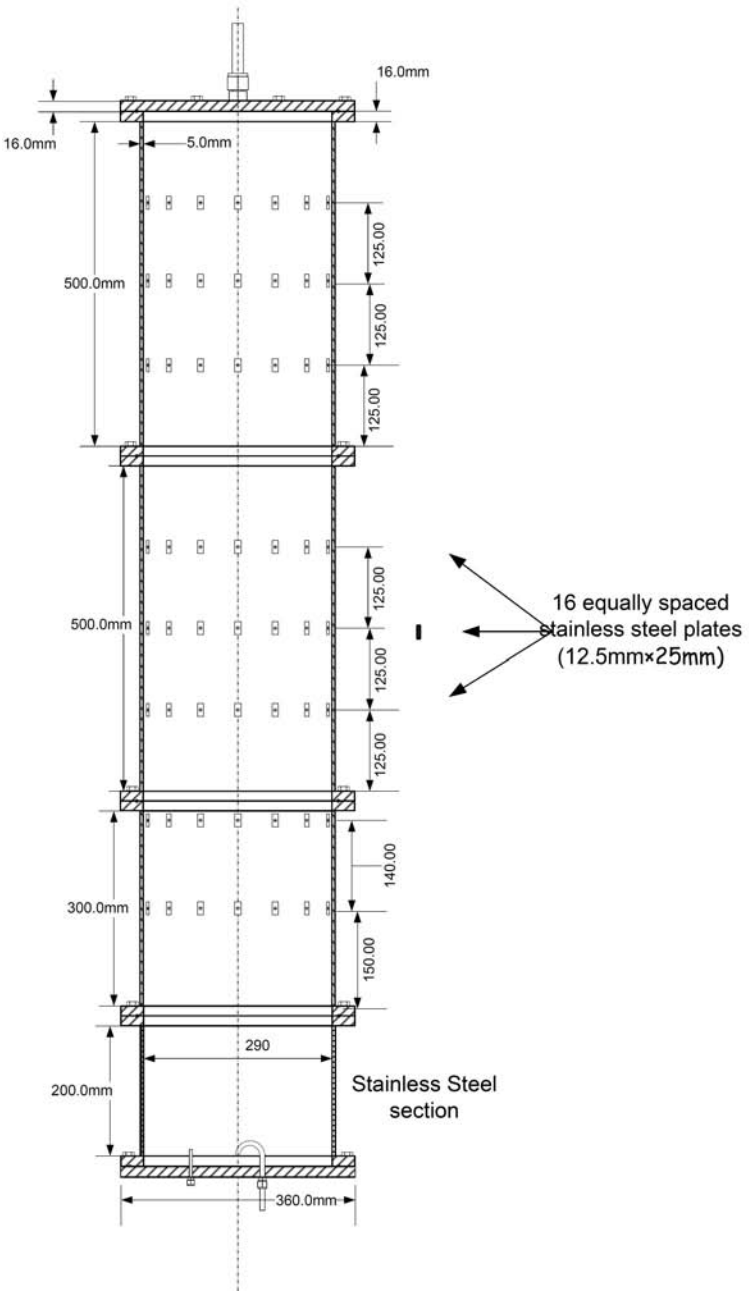

Figure 5.2: Mechanical drawing of the bubble column

It was decided to divide the perspex section into three parts for structural stability during transportation and for easy installation of the electrodes, as access to the inside of the middle of a long column would not have otherwise been possible. These perspex sections

and the one stainless steel section at the base are connected by flanges, which is shown in detail in Figure 6.2. A rubber O-ring is used in between the flanges to ensure there are no leaks.

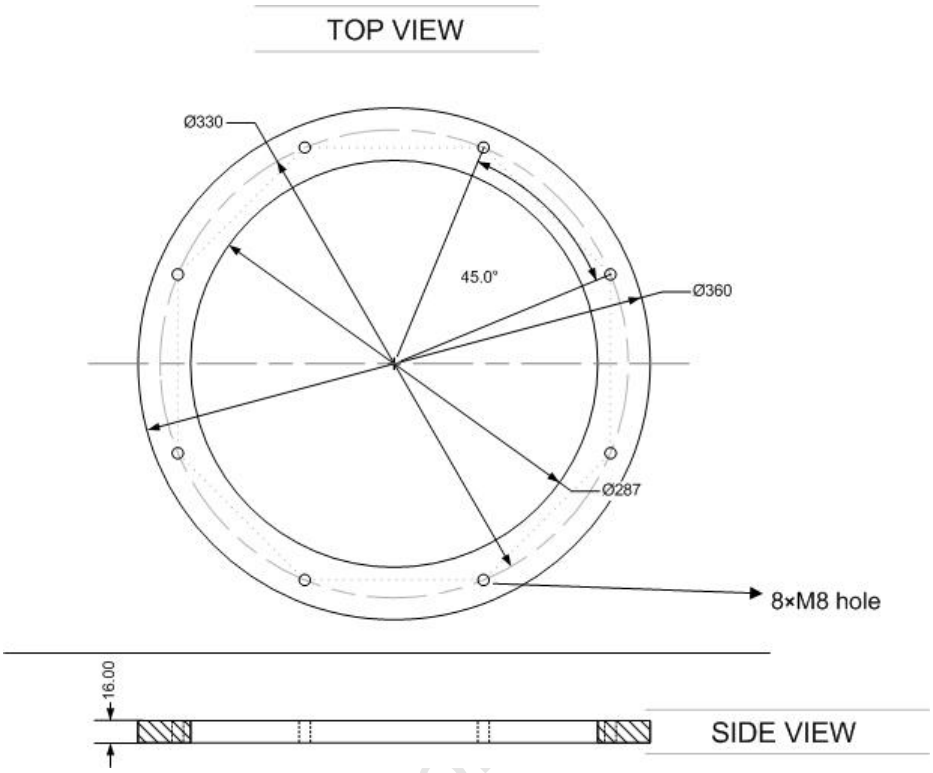

Figure 5.3: Mechanical drawing of a Perspex/stainless steel flange used to connect the column together

5.3 UCT Tomography Hardware System

Figure 5.4 shows the structure of an ERT system. From this it can be seen that there are two main components to the ERT hardware system - the sensors/electrodes and the data acquisition system. Both of these components are discusses briefly in the following sub-sections.

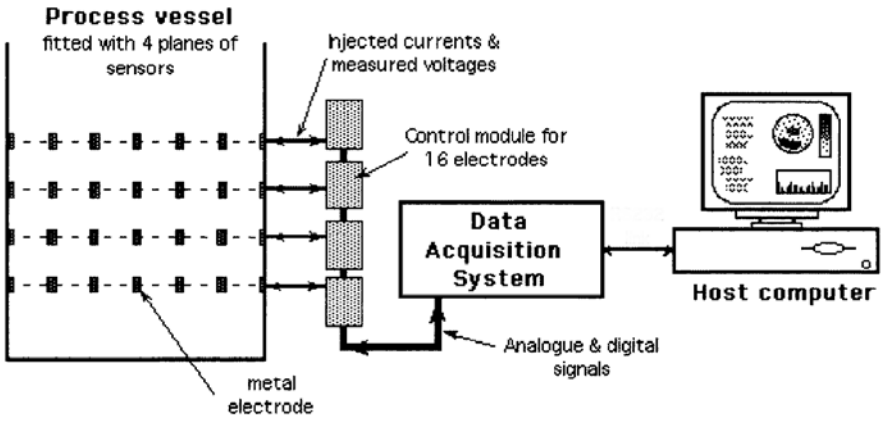

Figure 5.4: The structure of a typical electrical resistance tomography system, Dickin and Wang (1995)

5.3.1 Sensors/Electrodes

Unlike electrical capacitance tomography (ECT) systems, the sensing electrodes used in ERT must be in contact with the conductive medium within the process vessel. In addition, the sensors must be more conductive than the electrolyte in order to obtain reliable measurements (Deng et al. (2010)). For the majority of process applications, the electrodes are metallic and can be fabricated from stainless steel, silver, gold, platinum, silver, palladium or any suitable material exhibiting a number of properties. These properties include, in no inferred order of priority, low-cost, ease of fabrication and installation, good electrical conduction and resistance to abrasion and corrosion (Dickin and Wang (1995)). The electrodes are located equi-distantly around the process vessel to map resistivity changes across the plane or planes of interest. The positioning of the electrodes are important since the reconstruction algorithm assumes that the electrodes are located at precisely defined intervals. According to Dickin and Wang (1995), the positioning is somewhat less critical if the logged data are fed into a qualitative reconstruction algorithm, which is used to produced live images, since the logged data are normalized with respect to the reference data set prior to the reconstruction process. The quantitative algorithm, however, is highly sensitive to electrode placement problems because the data are not normalized prior to reconstruction.

The size of the electrodes is another important factor because consideration here is given to the widely used current-injecting and voltage-measuring ERT system. Consequently, a large surface area is required for the current-injecting electrodes to ensure that an even current density is generated within the vessel (Hua et al. (1993)). Correspondingly, in detecting the resultant equipotential, a small surface area, ideally a needle point, is optimal to avoid averaging several equipotentials. Ideally, the sensors used in ERT would be like those described either by Hua et al. (1993) or Paulson et al. (1992). Hua's electrode structure is shown in Fig.5.5 and is described as a compound electrode. Here the current source is fed to the relatively large outer surface area portion and the voltage measurement made via an insulated point-sized central electrode. The excessive amount of time required to construct and connect up a robust form of this type of electrode is at present prohibitive for many process tomography applications.

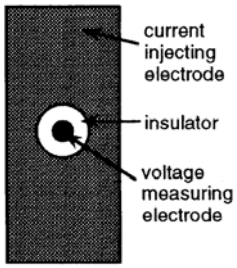

Figure 5.5: Ideal electrode sensor described by Hua et al. (1993)

The alternative approach, described by Paulson et al. (1992), employs differently sized electrodes for injection and measurement, as can be seen in Fig.5.6. The smaller point-sized measuring electrodes are interleaved between the larger current-injecting ones. This approach, however, requires twice the number of connectors, cabling and associated circuitry with identically sized electrodes throughout.

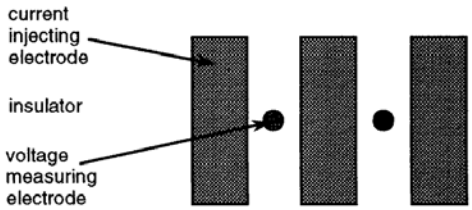

Figure 5.6: Ideal electrode sensor described by Paulson et al. (1992)

Despite these alternative configurations available, it has been decided, primarily for reasons of simplicity, to employ electrodes of identical sizes both for injection and for measurement in this thesis. Wang et al. (1995) developed a series of analytical and numerical models to investigate the error arising from employing larger electrodes for voltage measurement. Their conclusion, confirmed by Dickin and Wang (1995), was that the loss in measurement sensitivity as a result of using larger electrodes was minimal.

The electrodes were made from a stainless steel sheet as it has a high conductivity. The dimensions of the electrodes are 25mm in height, 12.5mm in width and a thickness of 1.5mm. These dimensions for the electrodes are scaled up from those used in a previous a PhD project, by Ryan Stevenson (2006), where similar elongated electrodes were used to account for the electric field bending in 3D, as well as to decrease the common voltage at the current driven electrodes, Wang et al. (1995). In the same thesis by Stevenson (2006), the connection of an electrode to the column using a screw (the 'connecting wire'), a nut and two rubber washers proved to be cumbersome, as numerous leaks occurred and silicone had to be used to seal the column. In this study the electrodes were placed in the same way except for two small rubber o-rings (2mm in thickness) being used instead of the rubber washers (as shown in Figure 6.3). This proved to be successful as once the construction of the columnn was complete, it was commissioned and pressure tested at 3 bar top pressure (applied at the top of the column through the vent pipe) and no leaks were observed.

5.3.2 Data Acquisition

The Electrical Resistance Tomography data capture system developed by Cilliers et al. (2001) at the University of Cape Town was used in the experiments conducted in this research. It is not the aim of the author to delve into a detailed description of the system, as it is beyond the scope of the thesis. Only a simple understanding of how the hardware operates is given. For a more technical description of the hardware system, please refer to the following papers by Wilkinson et al. (2003, 2005) and Cilliers et al. (2001).

The instrument utilizes a switched DC current pulse technique in conjunction with paral-

lel data acquisition to achieve the high data capture rates (up to a 1000 frames/second). The electrode layers installed on the bubble column consists of 16 uniformly spaced electrodes in which a single current source was multiplexed to the drive electrodes and the sense electrode pairs multiplexed to a single detector amplifier. This means that the current is injected into two electrodes (the drive electrodes), E1-E2, as shown in Fig.5.7(a) and the remaining electrode pairs, i.e. excluding any involving the injection pair (E2-E3, E1-E2 and E16-E1), measures the potential difference. This is then repeated for the next adjacent pair, E2-E3 (Fig.5.7(b)) of drive electrode and so on until the last pair (E16-E1), to complete one set of readings, resulting in 208 voltage measurements.

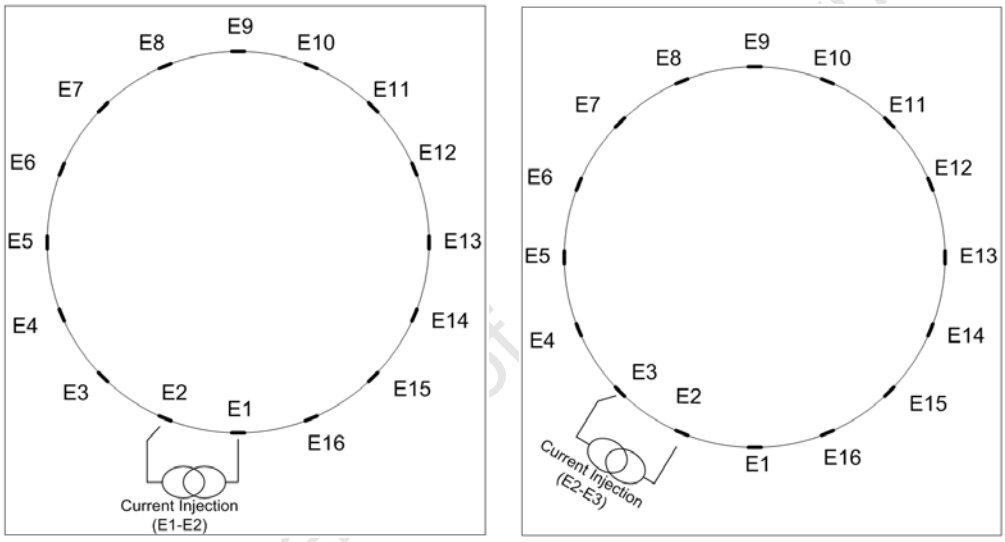

(a) Current injection to electrodes 1 and 2 (b) Current injection to electrodes 2 and 3

Figure 5.7: Current injection

The ERT instrument is controlled by a data capture and visualisation application developed by Long (2006). This software allows real time display of the conductivity profiles from multiple planes, as well as information on the measured voltages.

5.4 Electrode Design, Connection and Layout

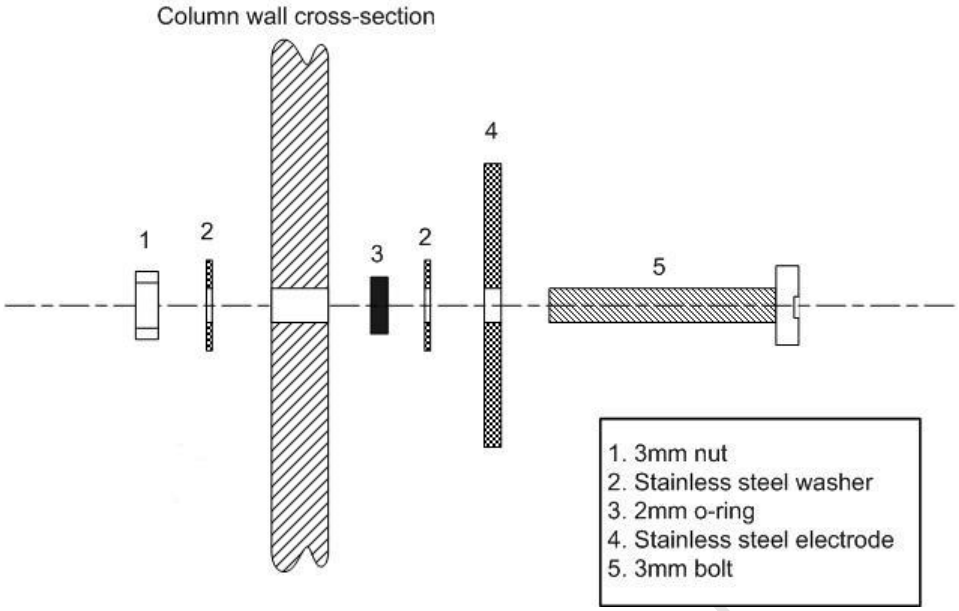

Figure 5.8: Schematic showing the connection of an electrode to the column

The layout of the 16-electrode layer is shown in Figure 6.4.

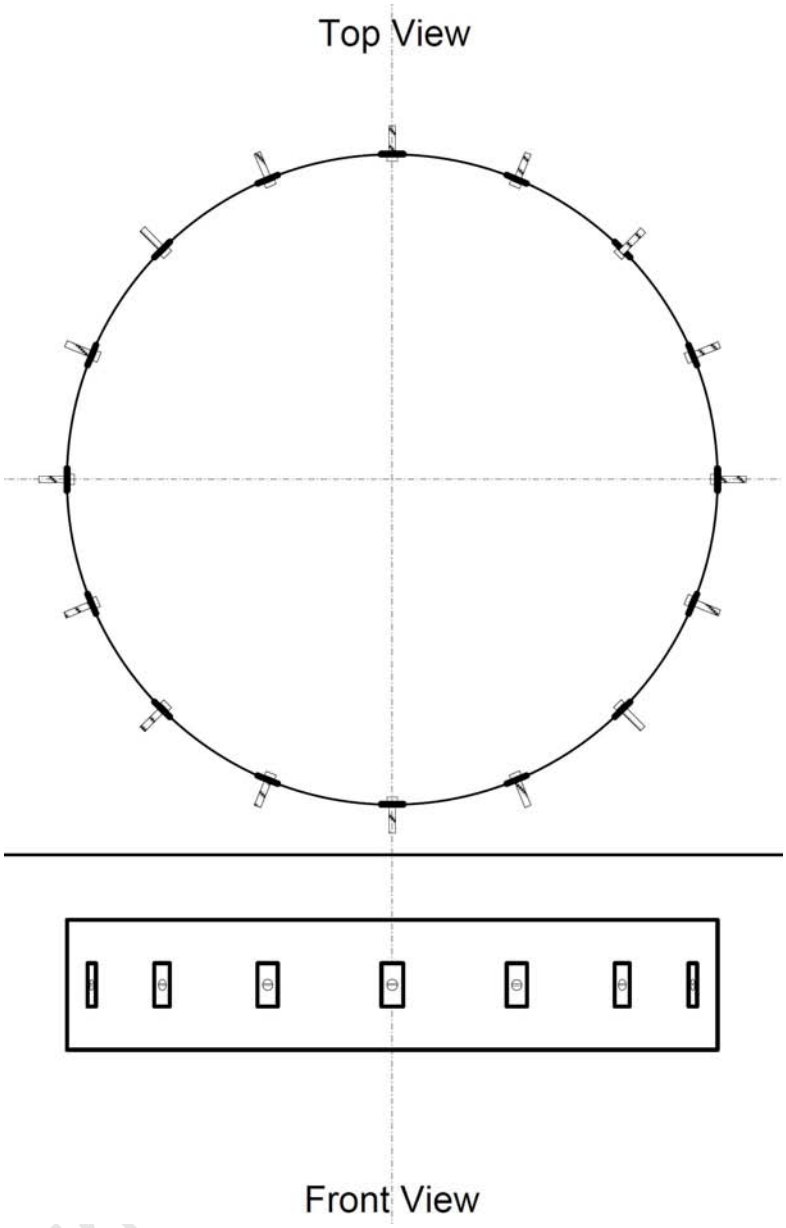

Figure 5.9: Layout of 16 electrodes in the column

5.5 Nozzle Designs

Four nozzles were tested using an air-water system. Each nozzle is made up of 1/4" stainless steel tubes. The design of the nozzle is shown in Figure 5.5.

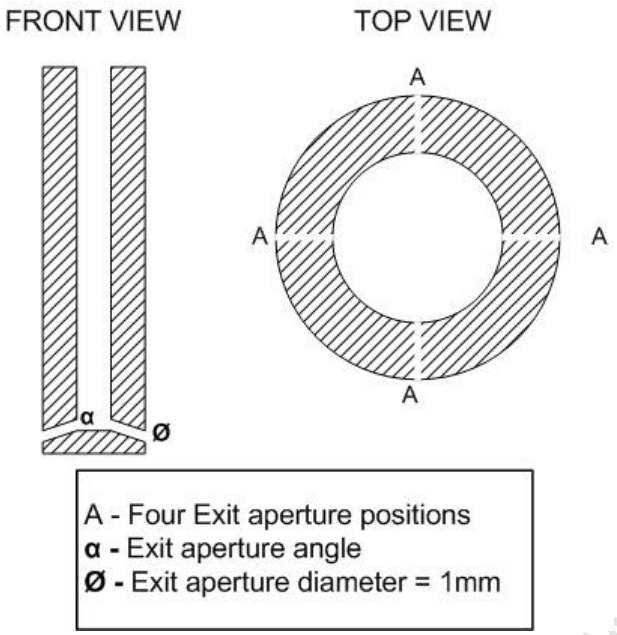

Figure 5.10: Design of a nozzle used in the experiments

The aperture angle of the nozzles, α, for the four nozzles are 10^o, 30^o, 45^o and 60^o. As describe earlier, these nozzles have been designed in such a way as to neutralise the formation of ice crystals during flashing. The nozzles are introduced from the bottom of the column with a 180^o bend to ensure that the reactant (air/butane) is introduced in a downward direction (shown in Figure 5.5), as the force at which gas hits the bottom of the column also assists in decreasing the formation of the ice crystals.

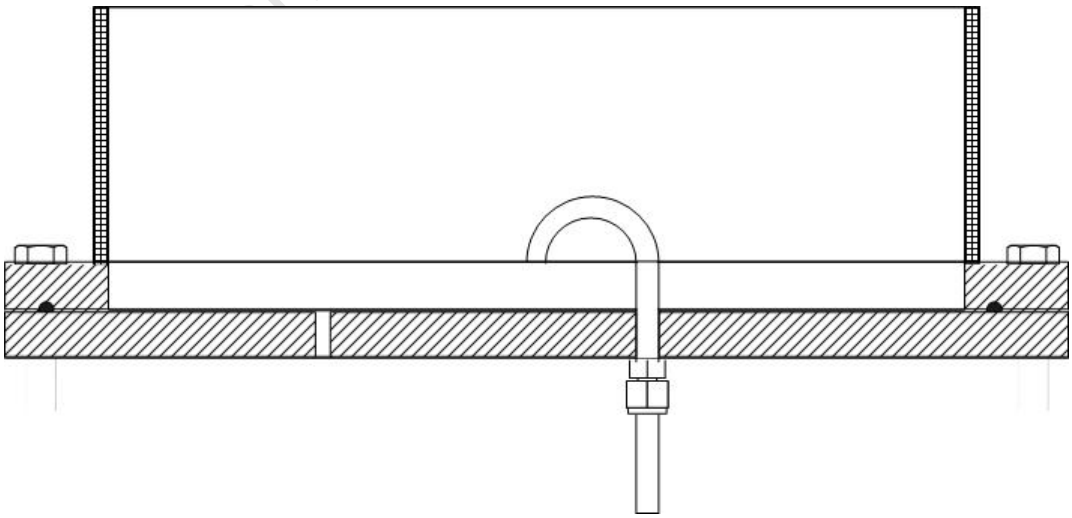

Figure 5.11: Direction in which the nozzle is placed in the column

5.6 Experimental Programme

The experimental programme initially consists of the system where air is passed into the column. The purpose of these set of experiments is to determine:

- firstly whether the gas hold-up obtained is of the same order of magnitude as those obtained in literature. This, along with the results from Chapter 6, will further validate the voidage results obtained using this ERT system.
- the influence of the nozzle aperture angle on the degree of mixing in the column and thereby determine the most optimised of the four nozzles.

The next set of experiments are to conduct the gaseous and liquid butane-water experiments to determine whether the flashing of the butane has a effect on the degree of mixing within the column.

5.6.1 Preparation of the Experimental Rig

- The bubble column is assembled together and the desired nozzle is fitted to the bottom of the column as shown in Figure 5.5.
- The nozzle is connected to the air/butane feed line system. Ensure that the feed pressure is consistently at 3barg to overcome any hydrostatic head pressure.
- Fill the column with water to about 3cm above the top electrode layer (about 1.5m in height). This will result in a height to diameter ratio of around 5, which is equivalent to that in industrial bubble columns.
- Fit the the top flange of the column and connect to the vent system to remove the air or butane.
- In the case of the liquid butane experiments, start-up the chiller and set to -15^oC.

5.6.2 Operation of a Single Run

- Start-up the ERT hardware system and the attached PC.

- Calibrate the voltage data. This is done by first taking 128 voltage readings (128 frames) with no current applied to the system, where no air is injected, and these frames are then averaged. The next step is to take 128 frames when current is applied. This allows for voltage reading offsets to be calculated, which is then applied to the readings obtained from the experimental runs.
- Open the air/butane valves. During the air-water experiments the flow is controlled using a rotameter and for the butane water experiments a Coriolis flow controller, which can also measure the density and temperature, is used.
- Once the required flow rate has been achieved, the rig is run for about two minutes to ensure steady state conditions are reached.
- Start the data capture and stop once approximately four minutes of data has been captured for each run.

5.6.3 Phase I - Air-Water System

The range of flow rates for the air-water experiments are shown in Table 5.1. These values have been chosen to give the same superficial gas velocities as that used in industry. Experiments using the above conditions will be conducted for each of the four nozzles and the radial gas hold-up profiles will be determined for each nozzle at each flow rate and at each electrode level to determine the degree of mixing.

Operating height of water level	Operating temperature of the water	Volumetric Flow rates of Air
$1.5m$	25^oC	$25lpm$ $30lpm$ $35lpm$ $40lpm$

Table 5.1: Operating Conditions for the Air-Water System

5.6.4 Phase II - Gas and Liquid Butane-Water Systems

The mass flow rates in the above table is equivalent to volumetric gas flow rates of $25lpm$ and $40lpm$ used in the air-water experiments. The temperature of the water in the column and that of the sub-cooled liquid butane were chosen such that a high temperature gradient exists between the two phases, which would result in instantaneous flashing occurring. The temperature of the water is heated up to and maintained at 55^oC using a heating jacket fitted at the bottom stainless steel section and a temperature controller. The sub-cooled butane at -5^oC is achieved by the use of a chiller.
The operating conditions for the butane-water experiments are shown in Table 5.2.

Operating height of water level	Operating temperature of the water	Mass Flow rates of Butane	Temperature of sub-cooled liquid butane
$1.5m$	55^oC	$0.063kg.min^{-1}$ $0.1kg.min^{-1}$	-5^oC

Table 5.2: Operating Conditions for the Air-Water System

The explosivity limits of butane is 1.9% - 9.0%. Looking at Table 5.2 the highest flowrate of butane, the concentration of butane is 1.06% resulting in a safe operating environment.

The next step is to validate the ERT system fitted on the rig and this is described in the following chapter.

Chapter 6

Validation of ERT Measurement

Non-conductive objects of known geometry and attenuation properties are classically used to validate the results obtained from the ERT reconstruction. In the context of Electrical Resistance Tomography, these non-conductive objects are called physical phantoms. In this chapter, we attempt to quantify voidage estimation error by the introduction of physical phantoms.

6.1 Voidage of Perspex Rod (Phantom) in a 290mm ID Column

A 54mm diameter perspex rod was inserted in the middle of the column and an ERT image was obtained. The same rod was also inserted closer to the wall and another image was reconstructed. These two images are shown in Figures 6.16.1(a) and 6.1(b).

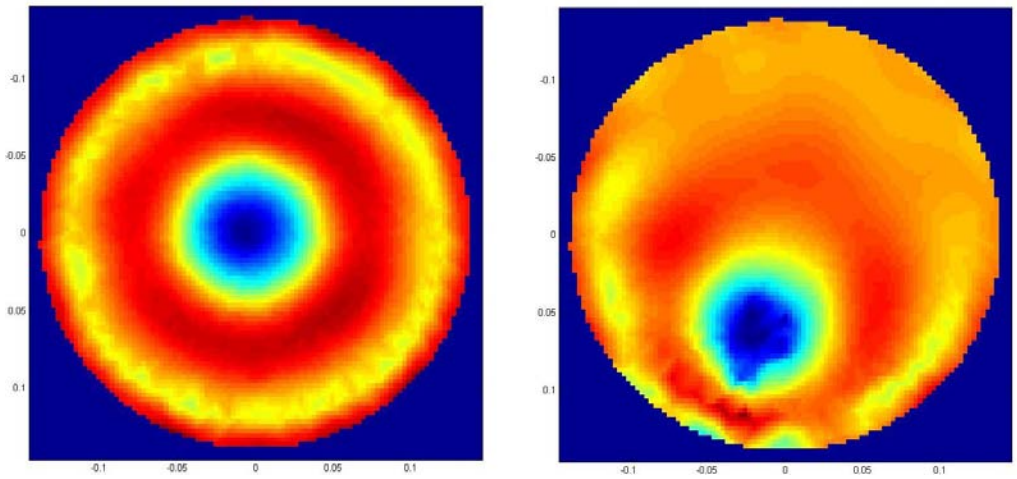

(a) Rod inserted in the middle of the column (b) Rod inserted close to the column wall

Figure 6.1: Images obtained by inserting 54mm diameter Perspex Rod

The actual voidage of a cross-section occupied by the rod is, $\frac{54^2}{290^2} = 3.5\%$ which is calculated by obtaining the percentage of the cross-section of the rod occupying the cross-section of the column. The voidage obtained from the tomography reconstruction is shown in the Table 6.1.

54mm Perpex Rod	Voidage (ε)	Absolute Error (%)
Actual Voidage	3.5%	-
Rod Inserted in the Middle	4.1%	0.6%
Rod Inserted Close to the Wall	3.8%	0.3%

Table 6.1: Voidage of 54mm Perspex Rod in the Column

The errors in both cases are not significant meaning that a more complicated system of phantoms can be used to test the ERT reconstruction. There is however a slightly increased error for the rod placed in the centre of the column, as opposed to that placed close to the wall. This is due to the fact that in the latter case, there is a greater sensitivity towards changes in the boundary voltages for a non-conducting phantom near an electrode which results a more accurate image. This finding has also been reported by Fransolet et al. (2002).

6.2 Voidage of Spherical Phantoms in a 290mm ID Column

The above study with the rods may not be reflective of the case when round gas bubbles move through the column. Therefore the purpose of this study is to illustrate the voidages obtained by the ERT method using spherical phantoms similar in shape to gas bubbles. Glass marbles, 34mm in diameter, were placed inside the column in the same plane as that of an electrode layer. This was achieved by hanging the marbles on very thin electro-neutral lines. Initially an image was taken for a single marble. The number of marbles were then increased and the voidage for each experiment was obtained. Figure 6.2 and 6.3 shows the reconstructed image of suspending 1 and six marbles respectively. The low or non-conductive areas (refer to the blue regions) indicate the presence of the non-conductive marbles. Table 6.2 shows the results of the reconstruction on these suspensions. The error for the case where six marbles were suspended is much higher than for the other suspensions. This can be attributed to the fact that the sixth marble was surrounded by the other marbles which, due to the use of a smoothness constrained regularisation, will average out the conductivity distribution resulting in a poorer resolution.

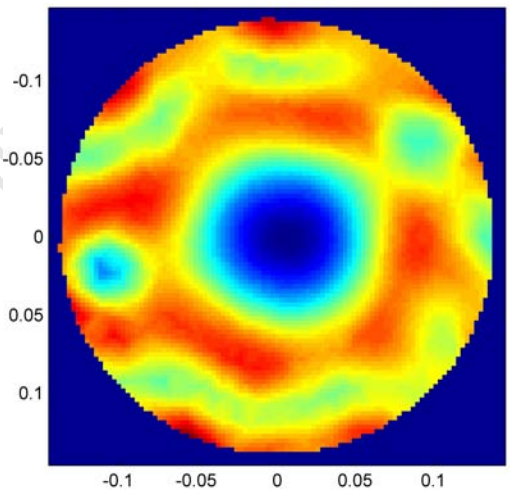

Figure 6.2: Reconstructed Image of 1 Spherical Suspended Phantom

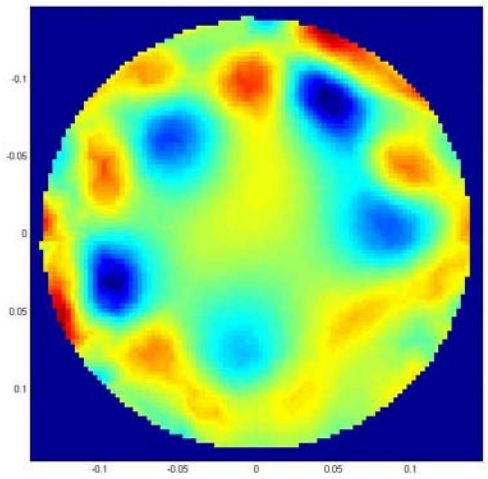

Figure 6.3: Reconstructed Image of Six Spherical Suspended Phantoms

No. of Spherical Phantoms (Marbles)	Actual Voidage (ε)	Voidage (ε)	Absolute Error (%)
1	1.46%	1.82%	0.36%
2	2.91%	2.40%	0.51%
3	4.37%	4.00%	0.37%
4	5.82%	6.56%	0.74%
5	7.28%	7.06%	0.22%
6	8.73%	7.12%	1.51%

Table 6.2: Voidage of 54mm Perspex Rod in the Column

Electrical resistance tomography is inherently a three-dimensional problem. However the two-dimensional voidage results shown in this chapter, validates the application of ERT for systems with water and gases in determining the gas hold-up of the latter phase.

Chapter 7

Degree of Mixing

In order to attain the objectives of this study, a method needs to be used or developed to quantitatively determine the degree of mixing that occurs in the bubble column. As described earlier in Chapter 2, the power law Equation 7.1 is used to characterise the radial gas hold-up profile in a bubble column. The higher the value of n, the steeper the profile is and therefore the better dispersed the gas is. This value of n can be used to quantify the degree of mixing of the gas phase in the bubble column.

$$\varepsilon_G = \widetilde{\varepsilon}_G \left(\frac{n+2}{n+2-2c} \right) [1 - c \left(\frac{r}{R} \right)^n] \tag{7.1}$$

The problem, however, with the above equation is that the radial gas hold-up profile needs to be parabolic in nature to get a good fit. The profiles obtained from the bubble column experiments conducted in this research are similar but not exactly parabolic in nature. This is shown in Figure 7.1(a) where the values of $\widetilde{\varepsilon}_G$, n and c are regressed.

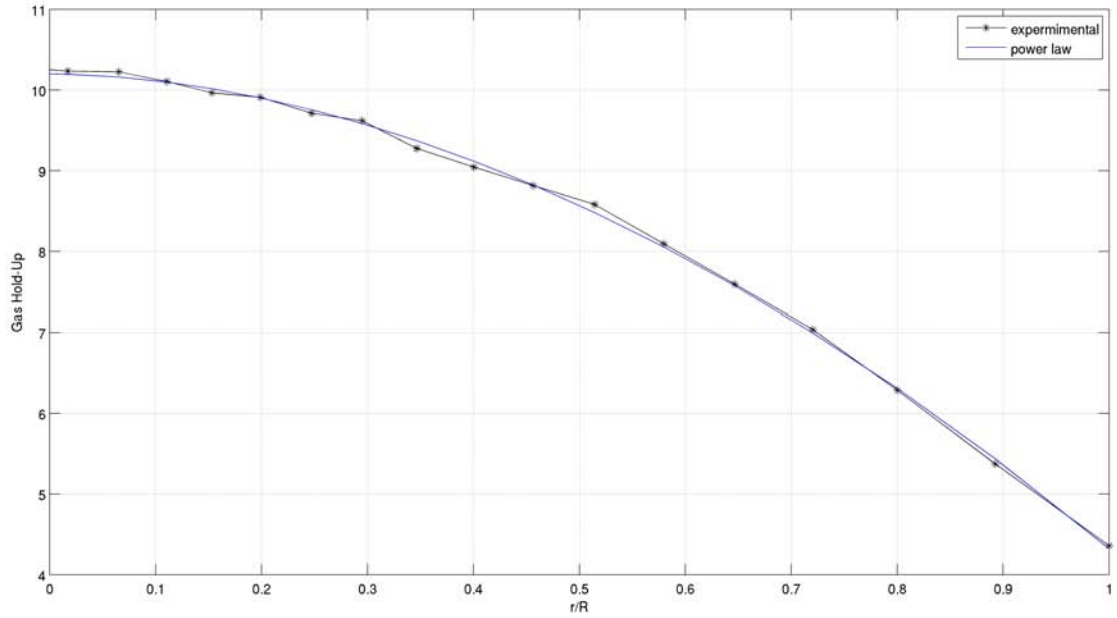

(a) Conventional 'nice' radial gas hold-up profile

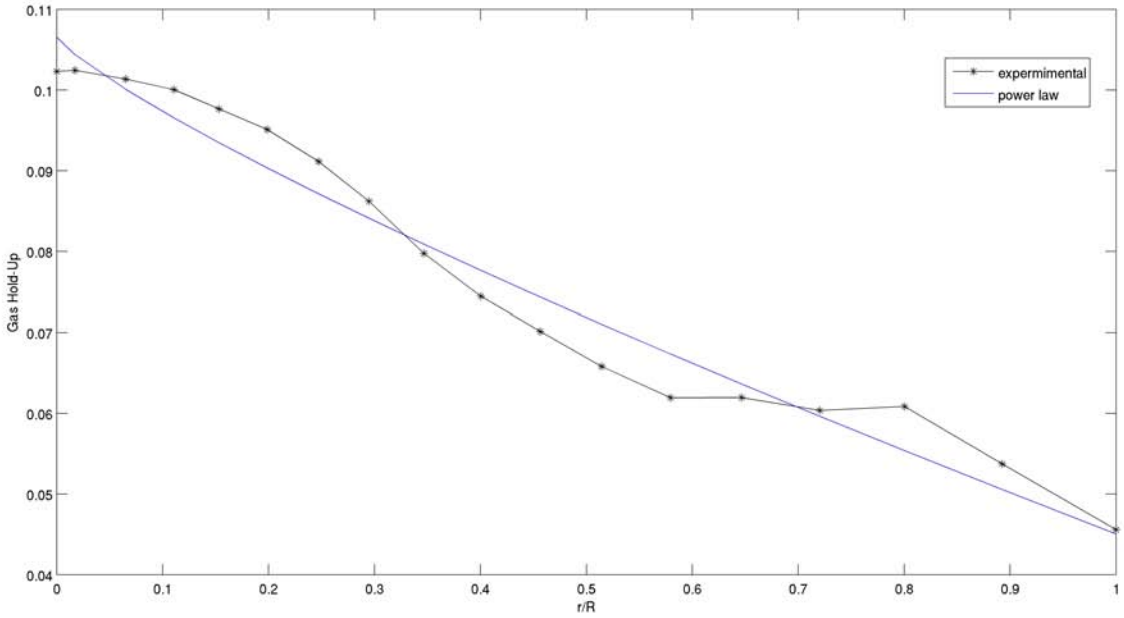

(b) Radial gas hold-up profile obtained from an ERT experiment

Figure 7.1: Comparison of power law equation fit to different radial gas hold-up profiles

Figure 7.1(b) shows that the power law equation cannot be used to quantify the degree of mixing of the gas phase in the bubble column for all of the radial profiles obtained from the experiments. A new method to quantify the dispersion for radial profiles therefore

needs to be developed. An effective and novel way to do this is to simply calculate the variance of the radial gas hold-up profile. The variance will be a measure of the degree of mixing. If we get a high concentration of bubbles at one point on this line, then we have a low voidage variance. On the other hand, if the bubbles are found to be well dispersed along the line, then the voidage variance would be high. As such, variance of the radial gas hold-up profile, when determined mathematically, is a reliable indicator of dispersion and hence of degree of mixing. Such a definition therefore helps us summarise all the information obtained from ERT. The variance of a random variable x, is calculated by Equation 7.2:

$$V(x) = \int (x - \mu)^2 \, p(x) \, dx \tag{7.2}$$

where
- $p(x)$ is the probability density function
- μ is the expected value of x and is equal to $\int x \, p(x) \, dx$

In order to use Equation 7.2 the radial gas hold up profile at an electrode layer plane needs to be determined. This is achieved by determining the conductivity distribution using the reconstruction algorithm. The cross-section of the column is then divided into 20 equally spaced concentric circles and the average conductivity is calculated in each concentric circle. The modified Maxwell equation (Equation 2.2) is used to find the average gas volume fraction (ε_g) in each concentric circle. This represents the average gas-hold at each radial point yielding the radial gas-hold-up profile, as shown by the 'Experimental' curve in Figure 7.1(b). The variance Equation 7.3 will now be as follows:

$$V(r_R) = \int (r_R - \mu)^2 \, p(r_R) \, dr_R \tag{7.3}$$

where
- r_R is the radius of a concentric circle divided by the column radius and normalised between 0 and 1
- $p(r_R)$ is the probability density function obtained by dividing radial gas hold-up profile by the area underneath it
- μ is the expected value of r_R and is equal to $\int r_R \, p(r_R) \, dr_R$

The above method was applied to radial gas-hold-up profile of parabolic in nature with varying width which are found in literature.. These radial profiles are shown in Figure 7.2. The 'widest profile showed a variance of 0.0827 and gradually decreases as the profile becomes narrower to a variance of 0.0594.

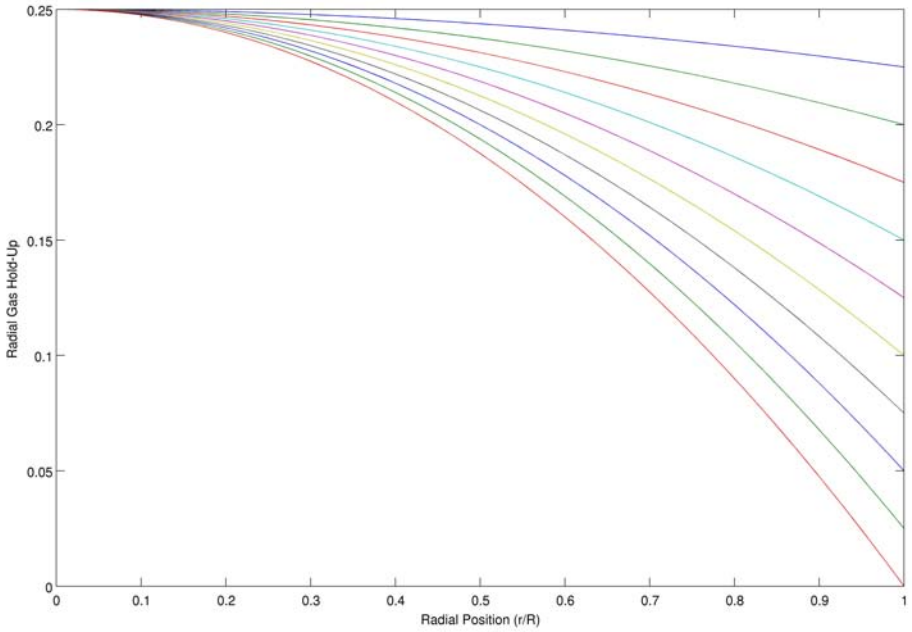

Figure 7.2: Comparison of variances obtained from parabolic radial gas hold-up profiles of varying width

This method was also applied to radial gas hold-up profiles that varied greatly from each other. These gas hold-up profiles are shown in Figure 7.3. In a perfectly mixed system the radial gas hold-up profile would be a flat line resembling a uniform distribution function. This type of a radial gas hold-up profile would have a variance of 0.0833 which equates to the highest possible degree of mixing. A degree of mixing (variance) of close to 0 suggests very poor or no dispersion of the gas has occured. In Figure 7.3 the profile depicting gas that is centrally distributed has a variance of 0.0025 showing less mixing. The normally distributed profile can be seen to be more distributed than the centrally distributed profile but less distributed than the uniform profile. This observation is quantitatively supported by itsvariance of 0.0145 which is inbetween the other two curves.

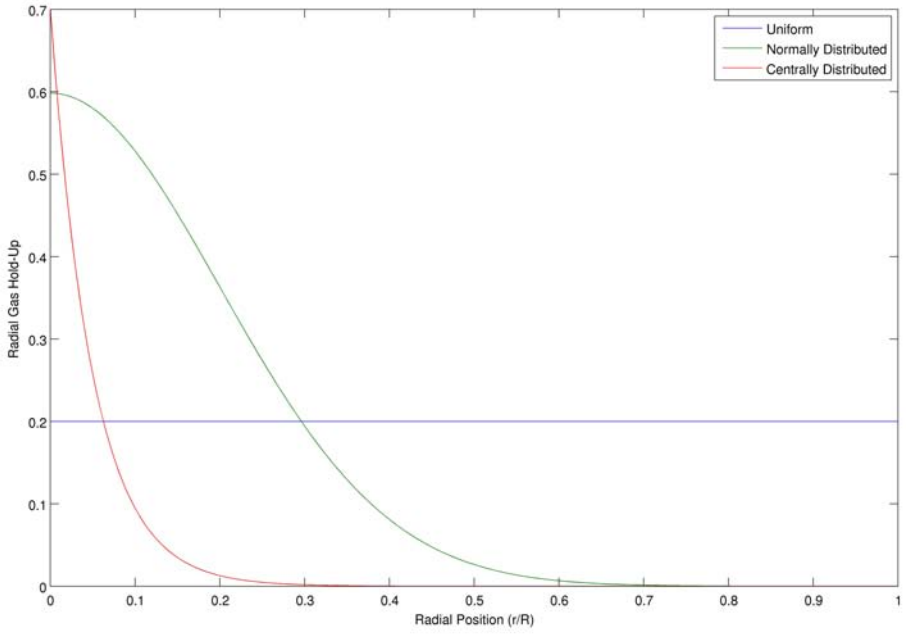

Figure 7.3: Comparison of variances obtained from different types of radial gas hold-up profiles

The method developed in this chapter has been shown to quantify the degree of mixing in the bubble column using the variance of radial gas hold-up profiles. This will then be used to find the optimal nozzle apperture angle and the effect onthe flashing of butane on the gas distribution within the column.

Chapter 8

Results and Discussion

8.1 Air-Water Experiments

The radial gas hold up profiles for the 10^o nozzle at each electrode layer is shown in Figures 10.3 - 10.10 in the Appendix. This shows that the radial gas hold-up profiles obtained from electrode layers 1 (Figure 10.3), 7 (Figure 10.9) and 8 (Figure 10.3) were found to be incorrect compared to the other layers. This can be attributed to the proximity of those layers to the bottom and top ends of the column. This results in cutting off or the blocking of the three-dimensional electric field generated at those layers by the bottom end, in the case of Layer 1, and the top end in the case of Layer 7 and 8 causing a change in the potentials at the periphery of the columns leading to incorrect conductivity distribution being obtained. It was decided that the results from these three layers will be omitted. The radial gas hold-up profiles for the middle layer (axial position of 0.83m) for each nozzle are shown in Figures 9.9 - 9.12 in the Appendix.

The method of variances that was described in the previous chapter is used to quantify these profiles into the degree of mixing in the air-water and butane-water systems. The results of the air-water system are shown in Figures 8.1-8.4.

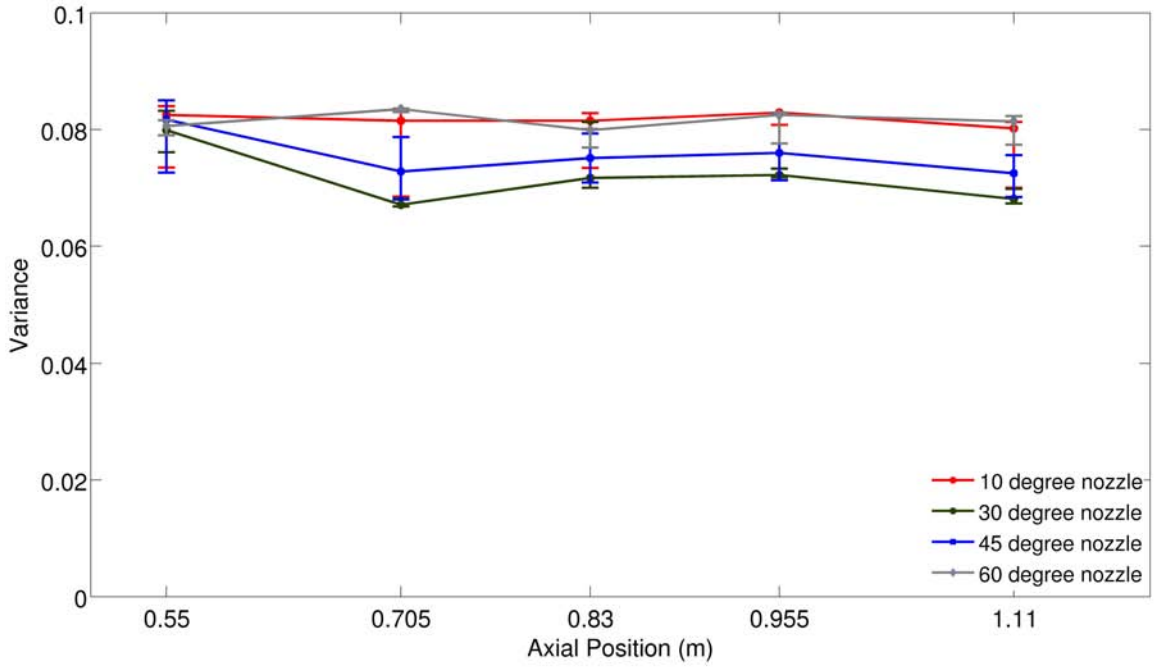

Figure 8.1: Variance of radial gas-hold-up distribution for each nozzle at air flow rate of 25 l/min

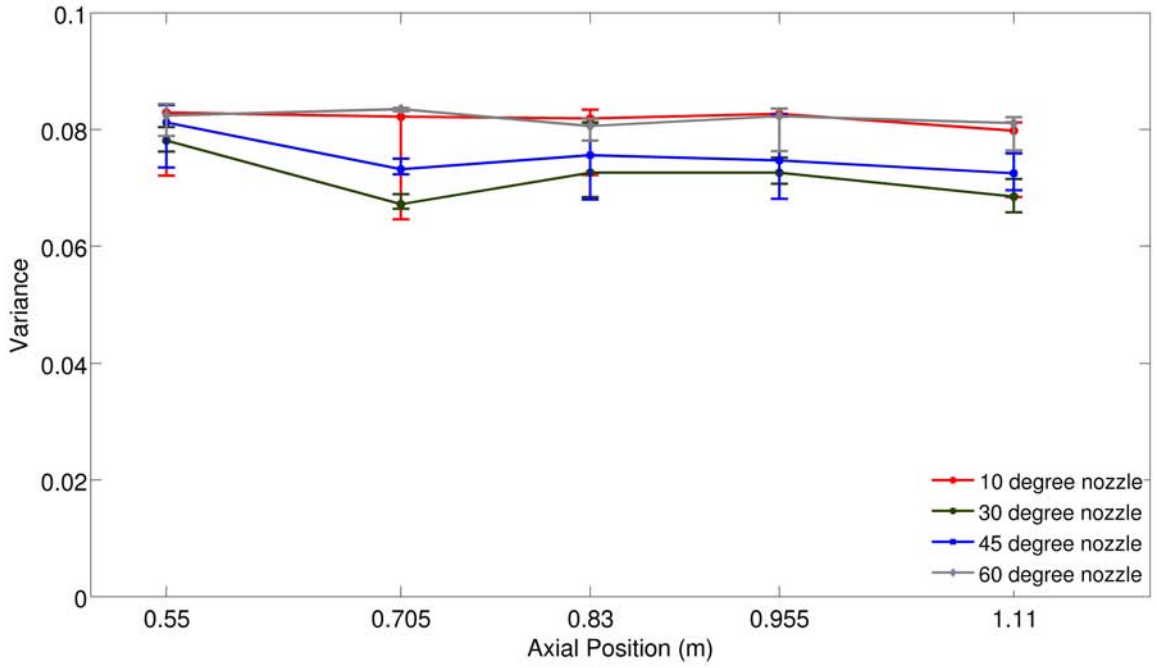

Figure 8.2: Variance of radial gas-hold-up distribution for each nozzle at air flow rate of 30 l/min

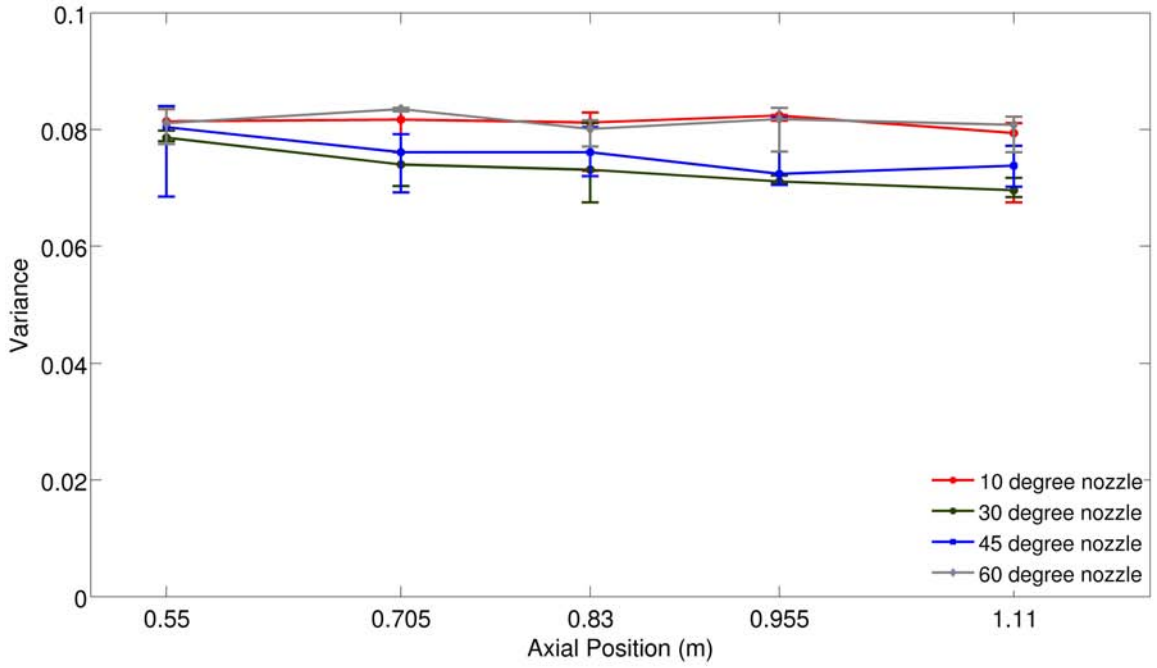

Figure 8.3: Variance of radial gas-hold-up distribution for each nozzle at air flow rate of 35 l/min

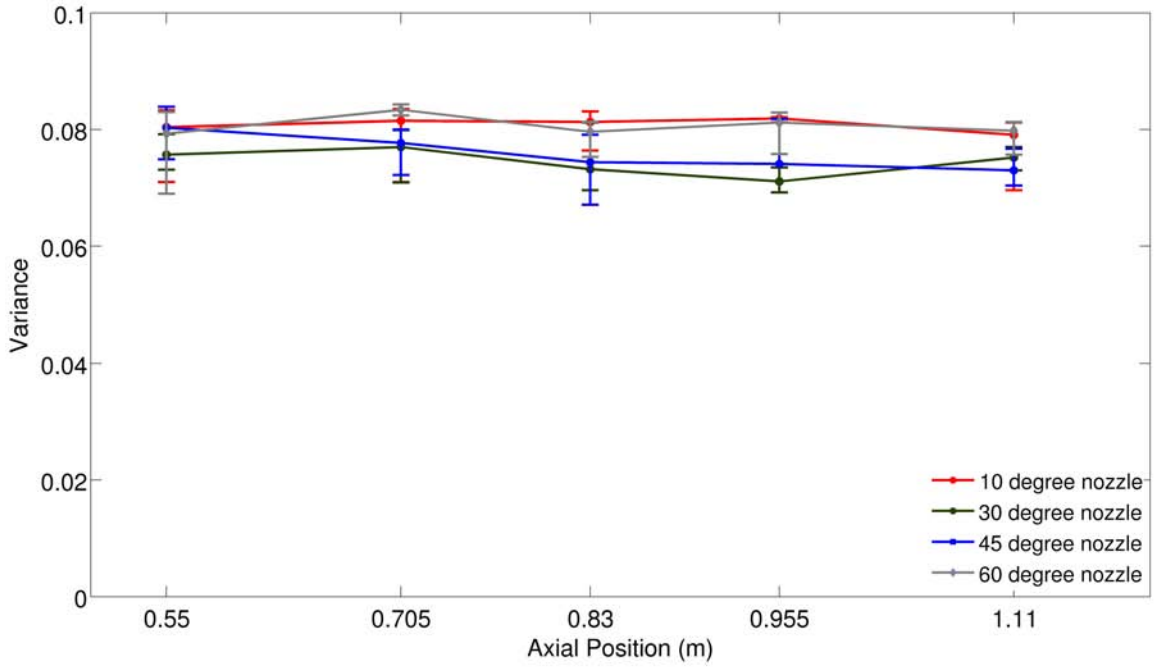

Figure 8.4: Variance of radial gas-hold-up distribution for each nozzle at air flow rate of 40 l/min

These figures show that at different axial positions there are slight changes in the degree of mixing at all air flow rates. However the error bars indicate that these changes in degree of mixing is insignificant for all four nozzles. In addition, as described in the previous chapter the highest degree of mixing possible is 0.0833 and the degre of mixing at all flow rates and at any axial position is around 0.08 meaning that with the current column dimensions and gas flow rates, for all four nozzles, the gas is well dispersed soon after introduction into the column and therefore an optimum nozzle aperture angle does not exist for a system with these design and operating parameters.

8.2 Butane Experiments

During the liquid butane experiments, the cooling of the butane to -5^oC was consistently achieved with the chiller and due to the low flow rates of the butane the temperature of the water was efficiently controlled at 55^oC. The results of the gaseous and liquid butane-water systems are shown in Figures 8.5 and 8.6.

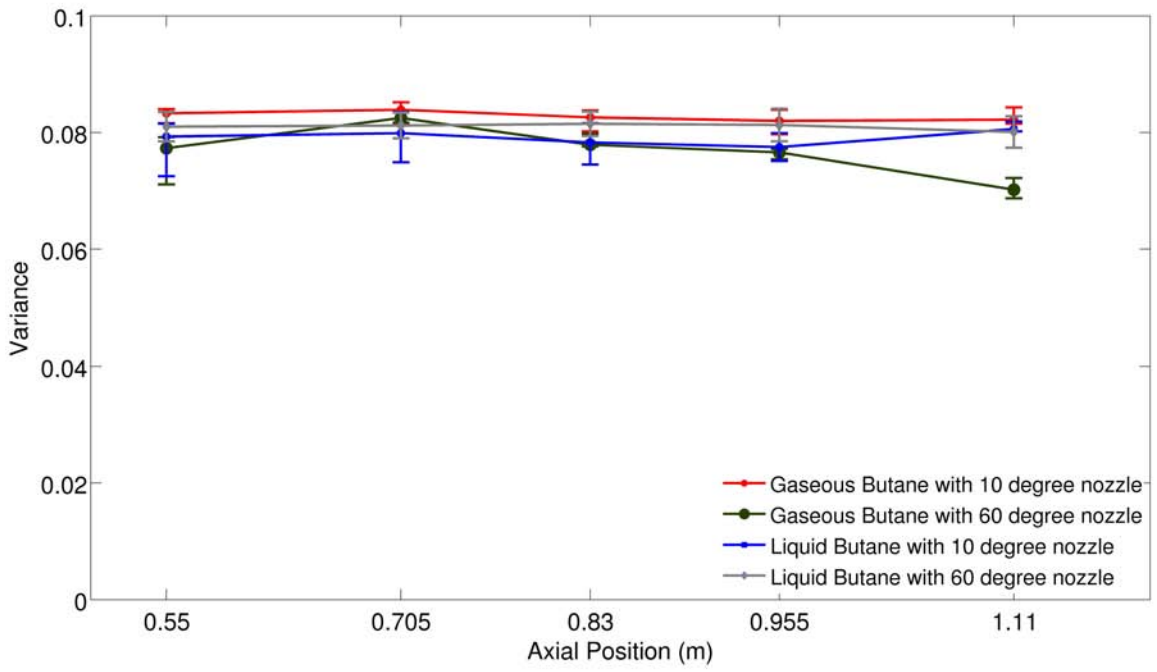

Figure 8.5: Variance of radial gas-hold-up distribution for each nozzle at butane flow rate of 25 l/min

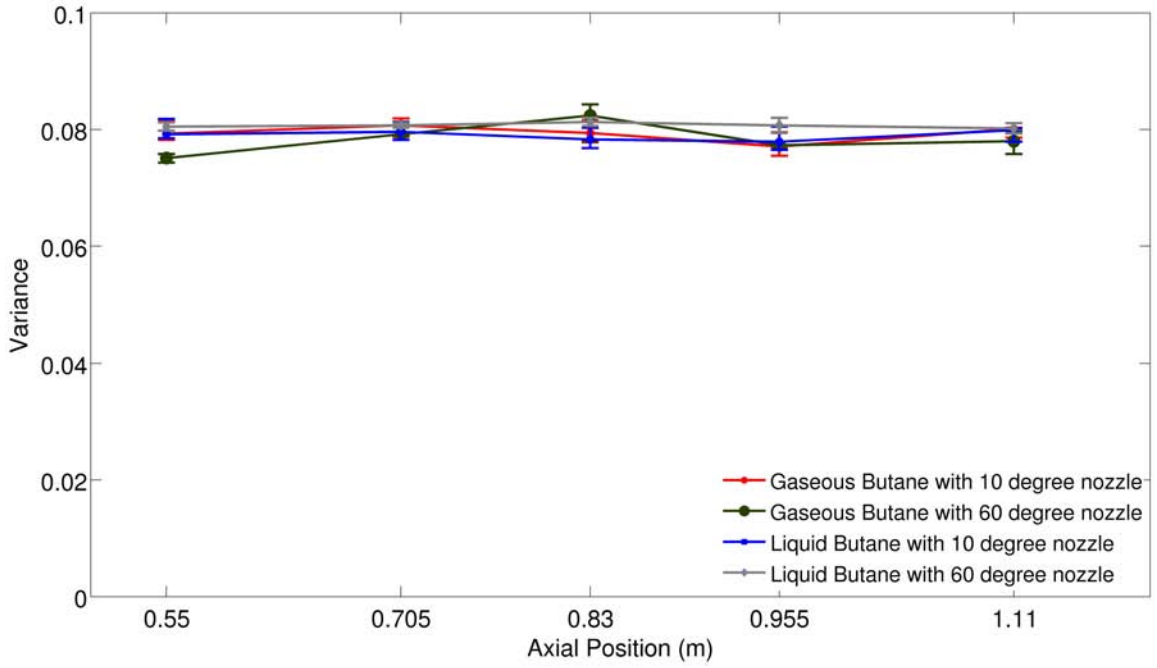

Figure 8.6: Variance of radial gas-hold-up distribution for each nozzle at butane flow rate of 40 l/min

The above figures show that there is no significant difference in the degree of mixing between the flashing and the non-flashing butane-water systems at any axial position for both the 10^o and the 60^o nozzles. This was to be expected, as from the air-water experiments, as well as the gaseous butane it can be seen that the gas phase is well dispersed soon after introduction, therefore any increase in the degree of mixing due to the flashing effect of the butane would be insignificant.

Chapter 9

Conclusions

This study has involved the analysis of the effect of nozzle geometry on the gas hold-up distribution in dynamic two phase systems. A fundamental yet simple model that was formulated showed that the inlet distribution of the gaseous phase can have and effect on the distribution of that phase in a bubble column. This warranted further investigation of the effect of these nozzles on the gas hold-up distribution. In order to achieve this, a bubble column was designed and constructed. Electrodes fitted to this column together with the UCT electrical resistance tomography (ERT) data acquisition system was shown to successfully obtain the conductivity distribution within the column. This conductivity distribution was then used to obtain the radial gas hold-up profiles in the column.

The use of variance, on the radial gas hold-up profiles, was used to quantitatively determine the degree of mixing in the column. This method was applied to the radial gas hold-up distributions obtained from the air-water and butane-water experiments. It was shown that in the bubble column with dimensions and inlet gas flow rates proportional to industrial conditions:

- In each of the four nozzles used in this study, the gas phase resulted in being well mixed immediately after introduction into the bubble column, meaning that the nozzles are well optimised for the current bubble column set-up.
- This therefore resulted in the flashing of the butane being insignificant with regards to its effect on the degree of mixing in the bubble column.

However this study has shown that the optimum design variables of a bubble column with regards to degree of mixing can be determined using ERT and the method of variance.

Bibliography

Bouaifi, M., Herbrard, G., Bastoul, D., Roustan, M., 2001. A comparitive study of gas hold-up, bubble size, interfacial area and mass transfer coefficient in stirred gas-liquid reactors and bubble columns. Chemical Engineering Processes 40, 97–111.

Bown, B. H., Barber, D. C., Wang, W., Lu, L., Leathard, L. H., Smallwood, R. H., Hampshire, A. R., Mackay, R., Hatzigalanis, K., 1994. Multi-frequency imaging and modelling of respiratory related electrical impedance changes. Physiological Measurement 15, 1–12.

Bukur, D., Daly, J., 1987. Gas holdup in bubble columns for fischer-tropsch synthesis. Chem Eng Sci 42, 2967–2969.

Burnett, D. S., 1987. Finite Element Analysis. New York, Addison-Wesley.

Cilliers, J. J., Xie, W., Neethling, S. J., Randall, E. W., Wilkinson, A. J., 2001. Electrical resistance tomography using a bi-directional current pulse technique. Measurement Science and Technology 12, 997–1001.

Clift, R., 1978. Bubble, Drops and Particles. Acadermic Press, London, 1st Edition.

Degaleesan, S., Dudkovic, M., Pan, Y., 2001. Experimental study of gas-induced liquid-flow structures in bubble colums. AIChE 47, 1913–1931.

Deng, X., Chen, Y., Yan, Z., Wei, Z., 2010. Ac impedance model of array electrodes in multisensor fusion system for two-phase flow measurement. IEEE Transactions on Instrumentation and Measurement 56, 1722–1726.

Dickin, F., Wang, M., 1995. Electrical resistance tomography for process applications. Measurement Science and Technology 7, 247–260.

D.N.Miller, 1980. Gas holdup and pressure drop in bubble column reactors. Ind Eng Chem Process Des Dev 19, 371–377.

Fish, J., Belytschko, T., 2007. A First Course in Finite Elements. New York, John Wiley and Sons.

Fransolet, E., Crine, M., L'Homme, G., Marchot, P., Toye, D., 2001. Analysis of electrical resistance tomography measurements obtained on a bubble column. Chemical Engineering Science 60, 6118–6123.

Fransolet, E., Crine, M., L'Homme, G., Toye, D., Marchot, P., 2002. Electrical resistance tomography sensor simulations: comparison with experiments. Measurement Science and Technology 13, 1239–1247.

Fransolet, E., Crine, M., Marchot, P., Toye, D., 2005. Analysis of gas hold up in bubble columns with non-newtonian fluid using electrical resistance tomography and dynamic gas disengagement. Chemical Engineering Science 60, 6118–6123.

Herholtz, S., 2003. Image reconstruction on ert measurements on a settling process. Ph.D. thesis, Masters Thesis, University of Cape Town.

Hikita, H., Asal, S., Tanigawa, K., Segawa, K., Kitao, M., 1980. Gas holdup in bubble column. Chem Eng J 20, 59–67.

Holden, P. J., Mann, R., Wang, M., Dickin, F. J., Edwards, R. B., 1998. Imaging stirred-vessel macromixing using electrical resistance tomography. AIChE 44, 780–790.

Hua, P., Woo, E., 1990. Electrical Impedence Tomography. The Adam Hilger, Bristol: IOP Publishing Ltd.

Hua, P., Woo, E. J., Webster, J. G., Tompkins, W. J., 1993. Using compound electrodes in electrical impedance tomography. IEEE Transactions on Biomedical Engineering 40, 29–34.

Jin, H., Tong, Z., Yang, S., Wang, M., Williams, R. A., 2007. Profiles of gas holdup in a gas liquid countercurrent bubble column using electrical resistance tomography. 5th World Congress on Industrial Process Tomography, Bergen, Norway.

Joshi, J. B., Veera, U. P., Phanikumar, D. V., Prasad, C. V., Deshphande, N. S., Thakre, S. S., Thorat, B. N., 1998. Gas hold up structure in bubble column reactors. PINSA 64A, 441–567.

Kantari, N., Borak, F., Ulgen, K. O., 2005. Bubble column reactors. Process Biochemistry 40, 2263–2283.

Karamanev, D. G., Nikolov, L. N., 1992. Free rising bubbles donot obey newton's law for free settling. A. I. Ch. E. Journal 38, 1993–1997.

Kim, J. I., Lior, N., 1997. Some critical transitions in pool flash evaporation. International Journal of Heat and Mass Transfer 40, 2363–2372.

Krishna, R., Maretto, C., 1997. Gas holdup in slurry bubble columns: effect of column diameter and slurry concentrations. AIChE 43, 311–316.

Long, T. M., 2006. An on-line velocity flow profiling system using electrical resistanc tomography. Ph.D. thesis, Masters Thesis, University of Cape Town.

Luo, H., Svendsen, H. F., 1991. Turbulent circulation in bbble coumns from eddy viscosity distribution of single-phase pipe flow. Canadian Journal of Chemical Engineering 69, 1389–1394.

Luo, X., Lee, D. J., Lau, R., Yang, G., Fan, L., 1999. Maximum stable bubble size and gas holdup in high-pressure slurry bubble columns. AIChE 44, 665–685.

Magnaudet, J., Eames, I., 2000. The motion of high-reynolds-number bubbles in inhomogeneous flows. Annual Review of Fluid Mechanics 32, 659–708.

Nassos, G. P., Bankoff, S. G., 1967. Slip velocity ratios in an air-water system under steady state and transient conditions. Chemical Engineering Science 22, 667.

Paulson, K. S., Breckon, W. R., Pidcock, M. K., 1992. A hybrid phanton for electrical impedance tomography. Clinical Physics and Physiological Measurement 13, 155–161.

Pinheiro, P. A. T., Loh, W. W., Dickin, F. J., 1997. Smoothness constrained inversion for two-dimensional electrical resistance tomography. Measurement Science and Technology 8, 293–302.

Prakash, A., Margaritis, A., Li, H., 2001. Hydrodynamics and local heat transfer measurements in a bubble column with suspension of yeast. Biochemical Engineering 9, 155–163.

Qian, W., Milkereit, B., Grber, M., 2007. Borehole resistivity tomography for mineral exploration. 69th EAEG Meeting, 11-14 June , London, UK.

Schumpe, A., Grund, G., 1986. The gas disengagement technique for studying gas holdup structure in bubble columns. Can J Chem Eng 64, 891–896.

Shah, Y., Godbole, S., Deckwer, W. D., 1982. Design parameters estimations for bubble column reactors. AIChE 28, 155–163.

Shaik, A., Al-Dahhan, M. H., 2007. A review on flow regime transition in bubble columns. Internation Journal of Chemical Reactor Engineering 5.

Stanley, S. J., Hristov, H., Mann, R., Primrose, K., 2005. On reconciling tomographic measurements with a fluid mixing model for semi-batch operation of a stirred vessel. CJChE 83, 1–7.

Stevenson, R., 2006. Analysis of particle suspension and mixing in biological systems: An application of tomography. Ph.D. thesis, Phd Thesis, University of Cape Town.

Wang, M., Dickin, F. J., Williams, R. A., 1995. Group-node technique as a means of handling large electrode surfaces in electrical impedance tomography. Physiological Measurement 16, 219–226.

Wang, M., Dorwood, A., Vlaev, D., Mann, R., 2000. Measurements of gas-liquid mixing in a stirred vessel using electrical resistance tomography. Chemical Engineering Science 77, 93–98.

Warsito, W., Fan, L., 2001. Measurement of real-time flow structures in gas-liquid and gas-liquid-solid flow system usingg electrical capacitance tomography (ect). Chemical Engineering Science.

Wilkinson, A. J., Randall, E. W., Cilliers, J. J., Durrett, D., Naidoo, T., Long, T., 2005. A 1000 frames/second ert data capture system with real time visualization. IEEE Sensors Journal 5, 300–307.

Wilkinson, A. J., Randall, E. W., Durrett, D., Naidoo, T., Cilliers, J. J., 2003. The design of a 1000 frames/second ert data capture system and calibration techniques employed. In Proceedings of 3rd World Congress on Industrial Process Tomography, 504–509.

Wu, Y., Ong, B. J., Al-Dahhan, M. H., 2001. Predictions of radial gas holdup profiles in bubble column reactors. AIChE 56, 1207–1210.

Xie, Y., Notfors, C., Sun, J., Xin, K., Biswal, A. K., Balasubramaniam, M. K., 2010. 3d prestack beam migration with compensation for frequency dependent absorption and dispersion. 72nd EAGE Conference and Exhibition Incorporating SPE EUROPEC 2010, 14-17 June, Barcelona, Spain.

Appendix

Radial Gas Hold-Up Profiles

Radial gas hold-up profiles for the 10^o nozzle at each electrode layer in the air-water system

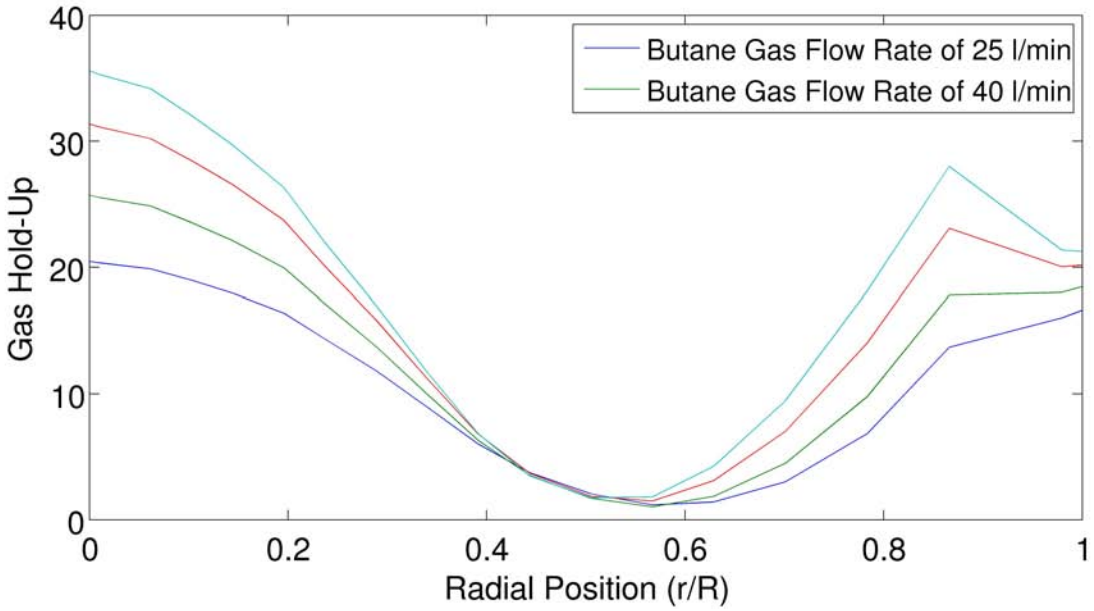

Figure 9.1: Radial gas hold-up profile at an axial distance of 0.38m

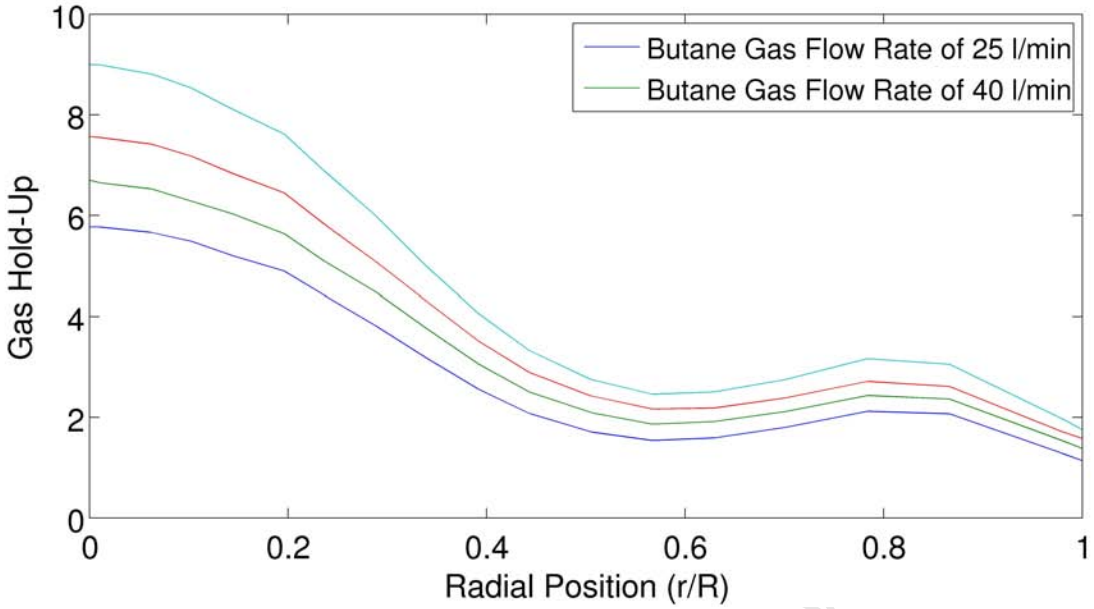

Figure 9.2: Radial gas hold-up profile at an axial distance of 0.53m

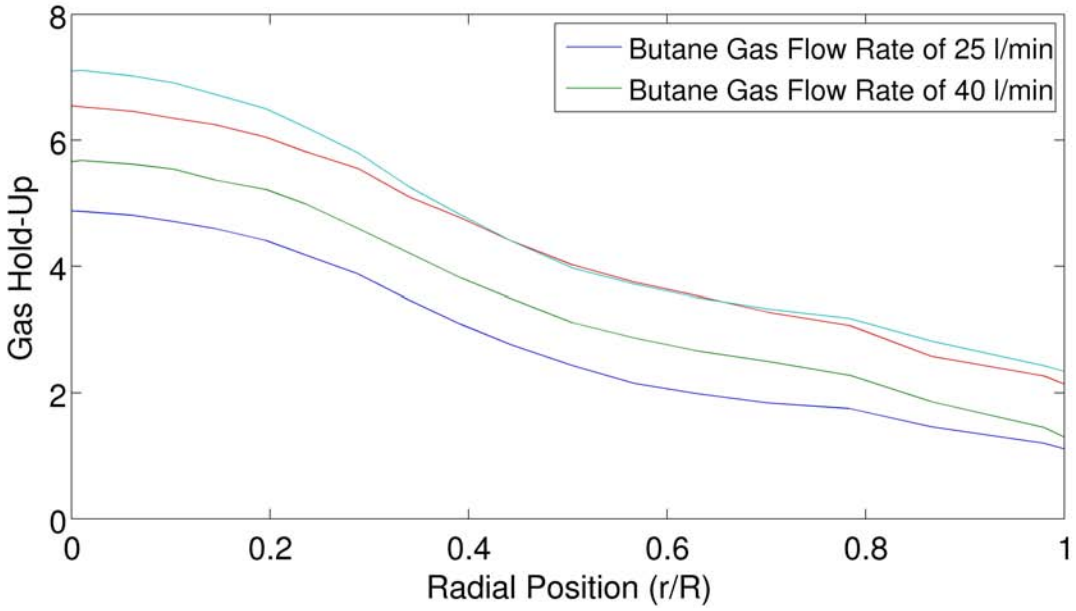

Figure 9.3: Radial gas hold-up profile at an axial distance of 0.70m

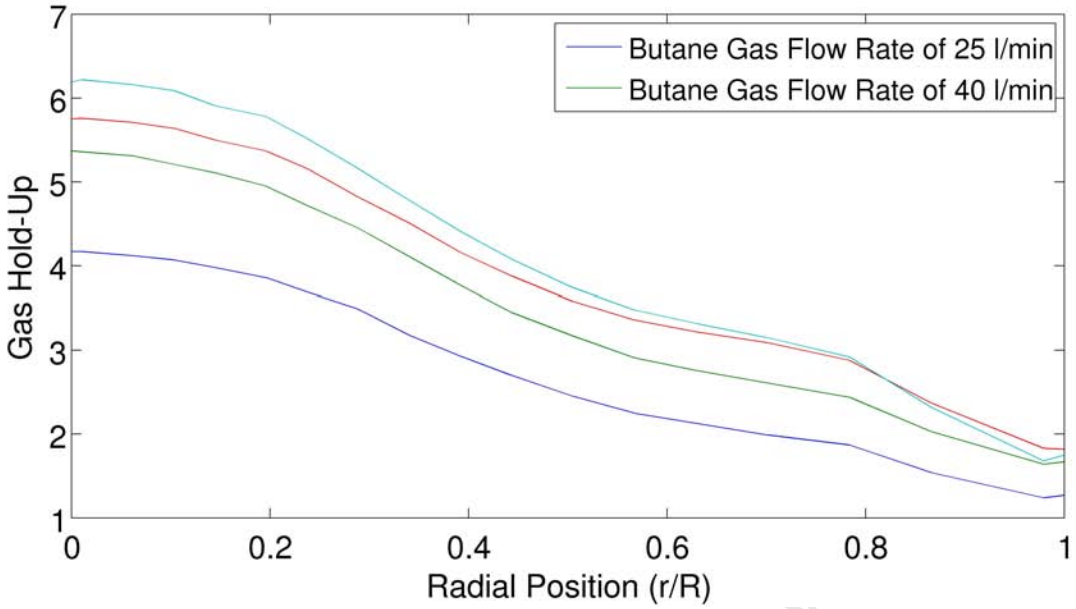

Figure 9.4: Radial gas hold-up profile at an axial distance of 0.83m

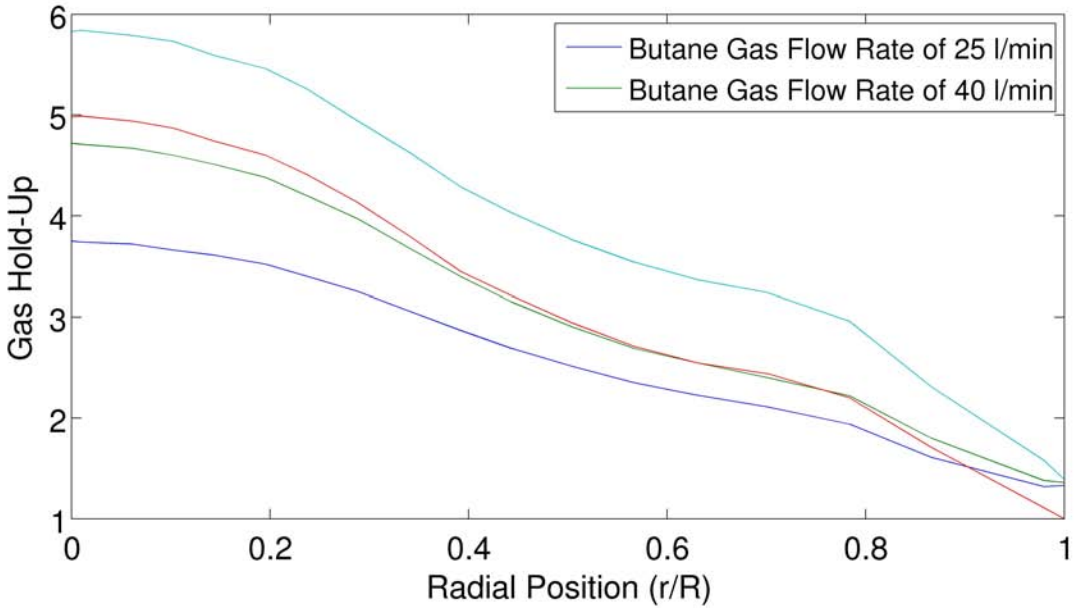

Figure 9.5: Radial gas hold-up profile at an axial distance of 0.95m

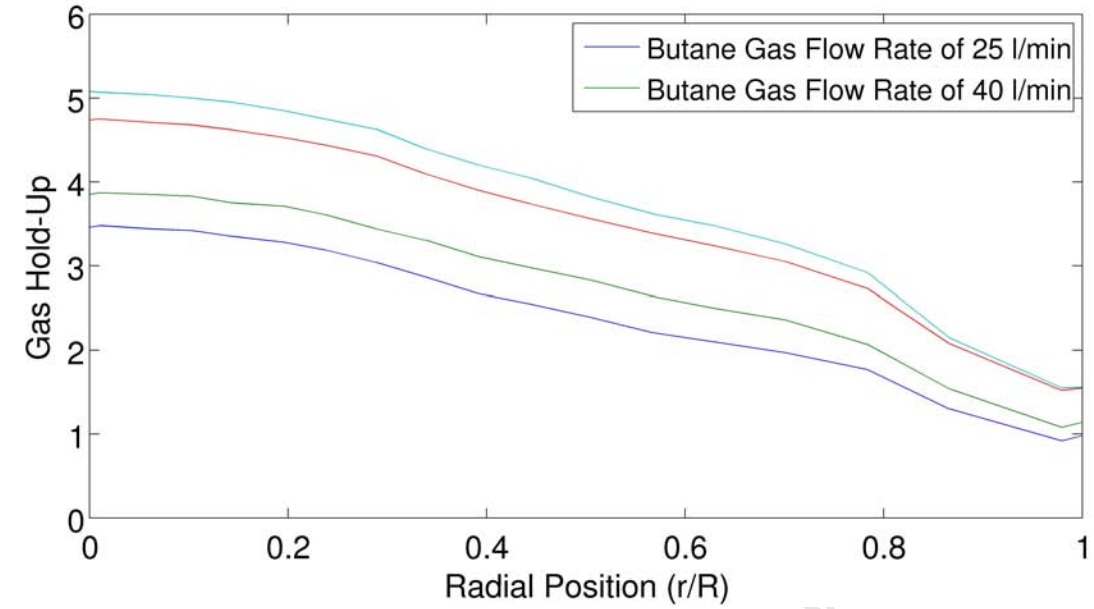

Figure 9.6: Radial gas hold-up profile at an axial distance of 1.11m

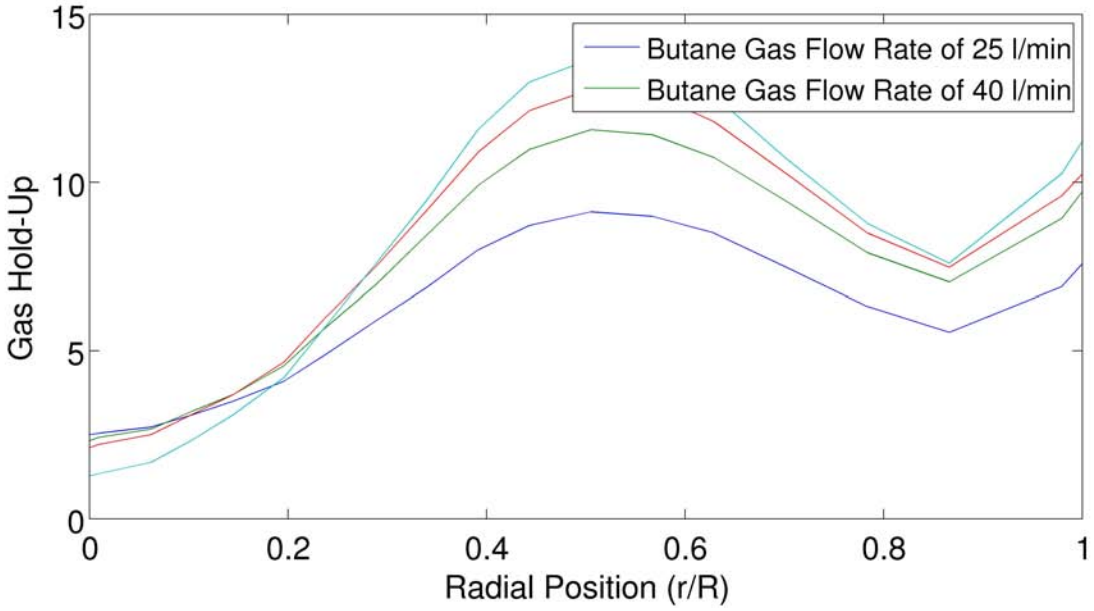

Figure 9.7: Radial gas hold-up profile at an axial distance of 1.33m

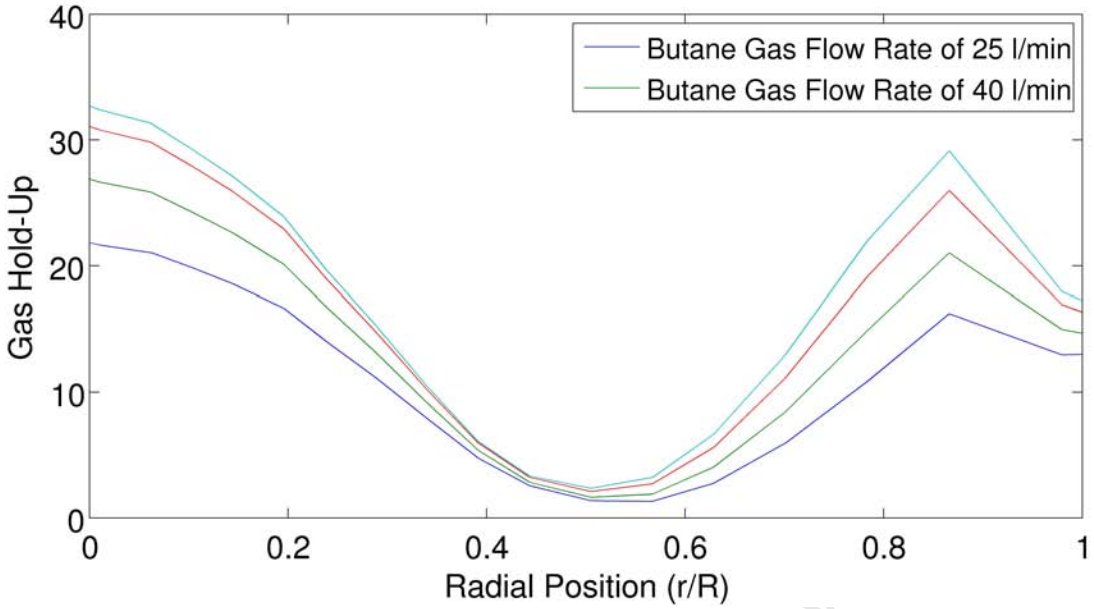

Figure 9.8: Radial gas hold-up profile at an axial distance of 1.45m

Radial gas hold-up profiles at the middle layer for each nozzle in the air-water system

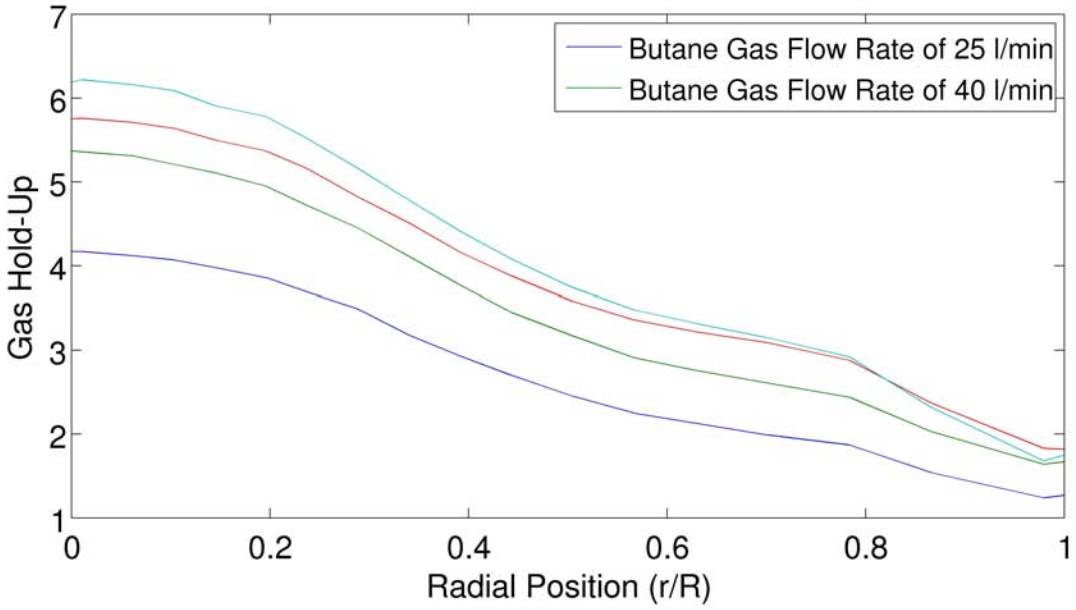

Figure 9.9: Radial gas hold-up profile at an axial distance of 0.83m using the 10^o nozzle

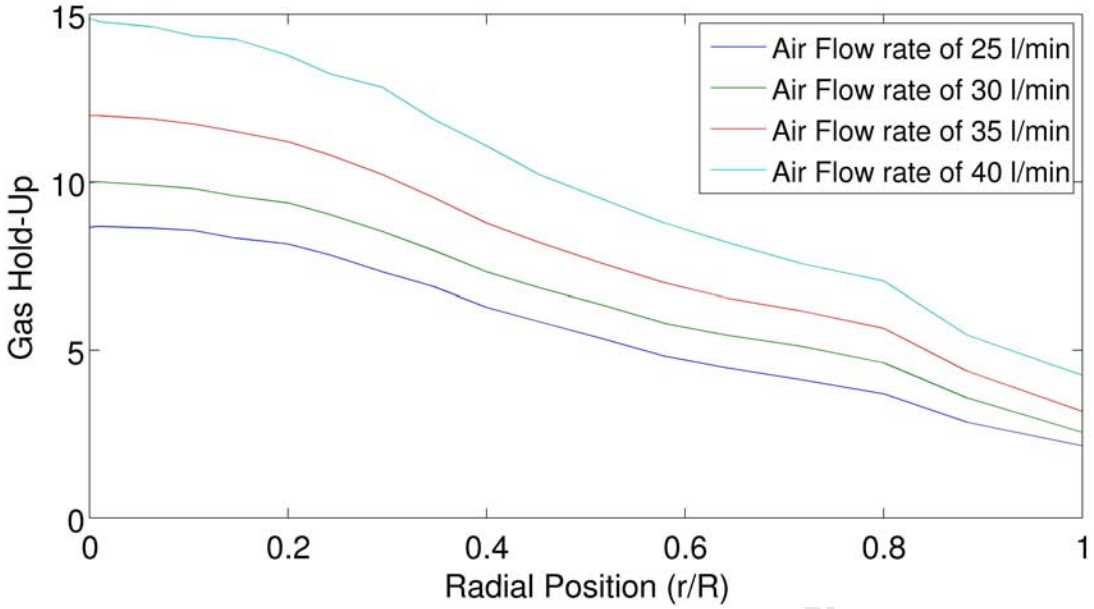

Figure 9.10: Radial gas hold-up profile at an axial distance of 0.83m using the 30^o nozzle

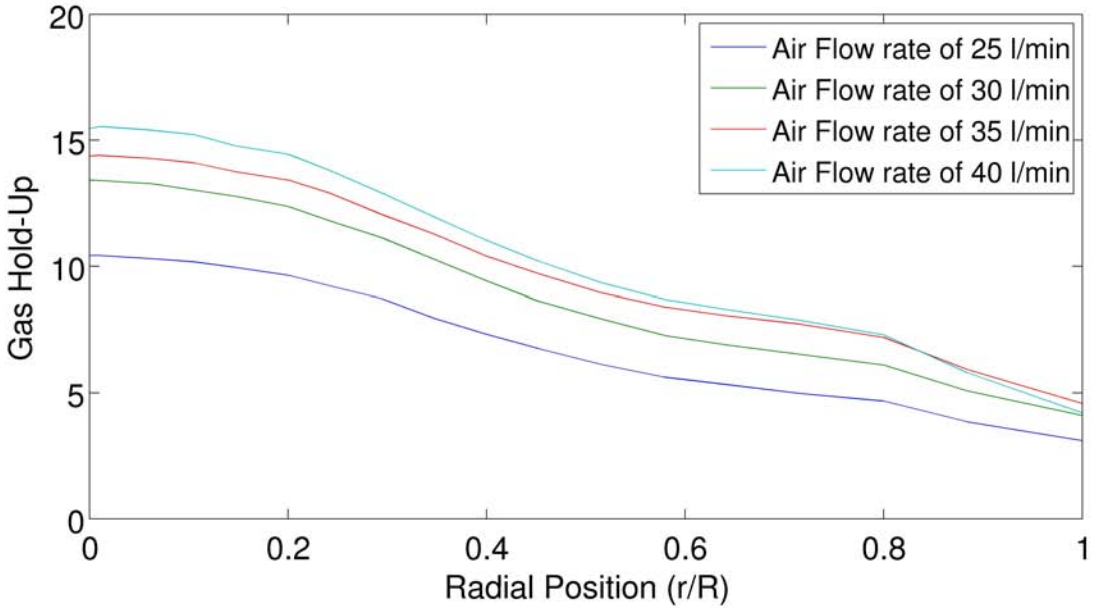

Figure 9.11: Radial gas hold-up profile at an axial distance of 0.83m using the 45^o nozzle

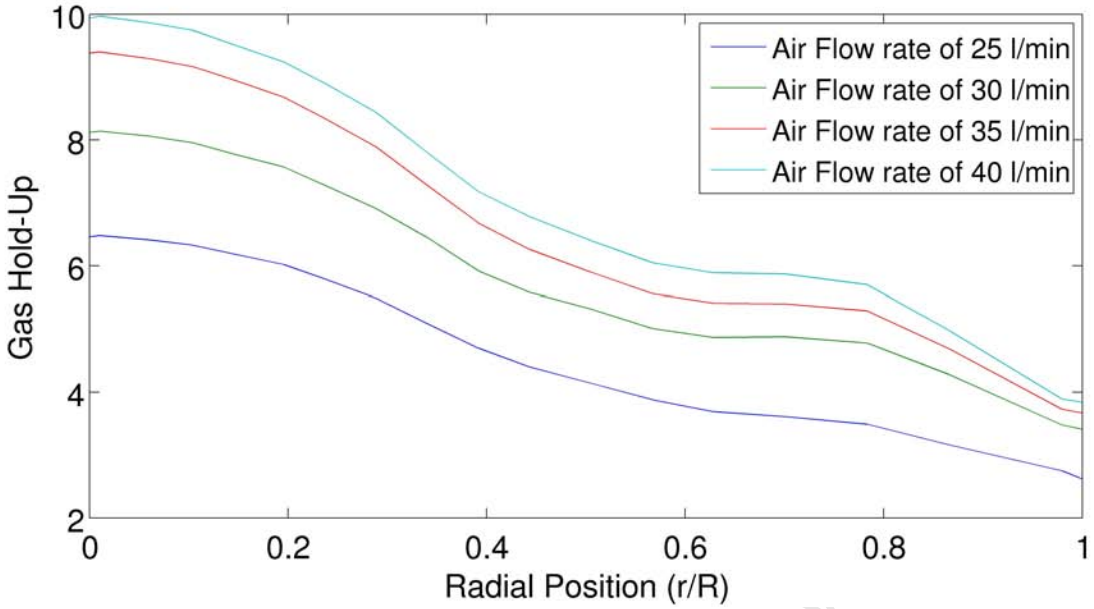

Figure 9.12: Radial gas hold-up profile at an axial distance of 0.83m using the 60^o nozzle

Air-Gaseous Butane Experiments

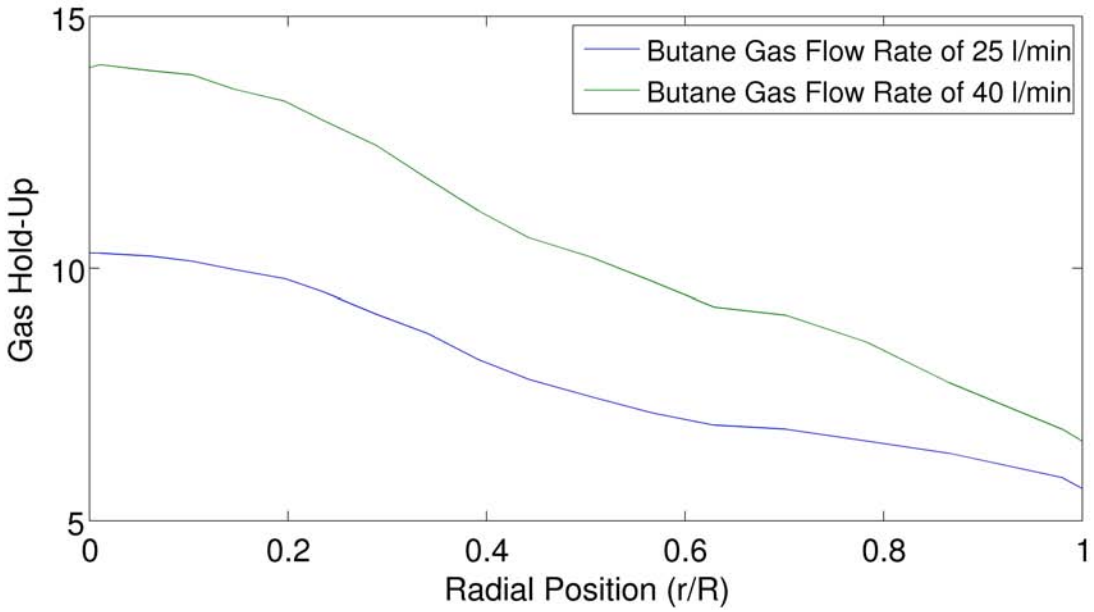

Figure 9.13: Radial gas hold-up profile at an axial distance of 0.83m using the 10^o nozzle

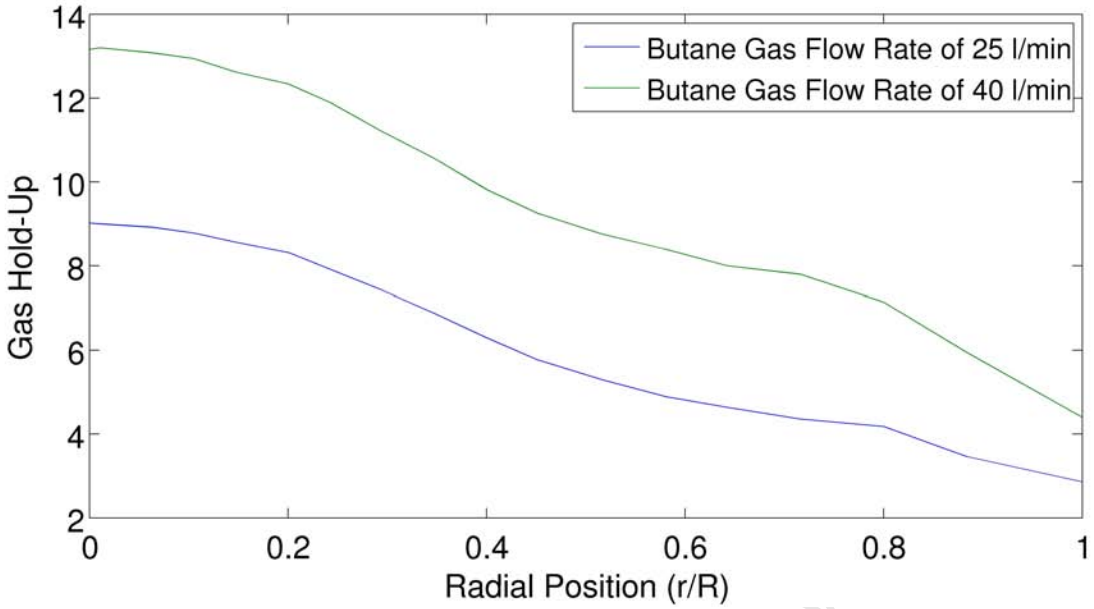

Figure 9.14: Radial gas hold-up profile at an axial distance of 0.83m using the 60^o nozzle

Air-Liquid Butane Experiments

Radial gas hold-up profiles at the middle layer for each nozzle in the gaseous and liquid-water system.

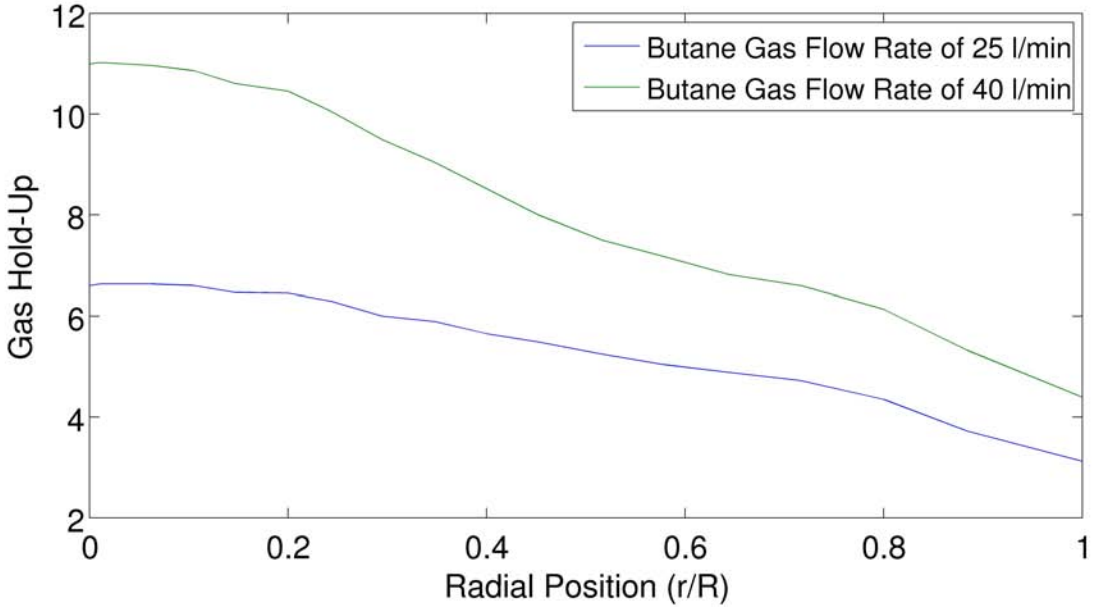

Figure 9.15: Radial gas hold-up profile at an axial distance of 0.83m using the 10^o nozzle

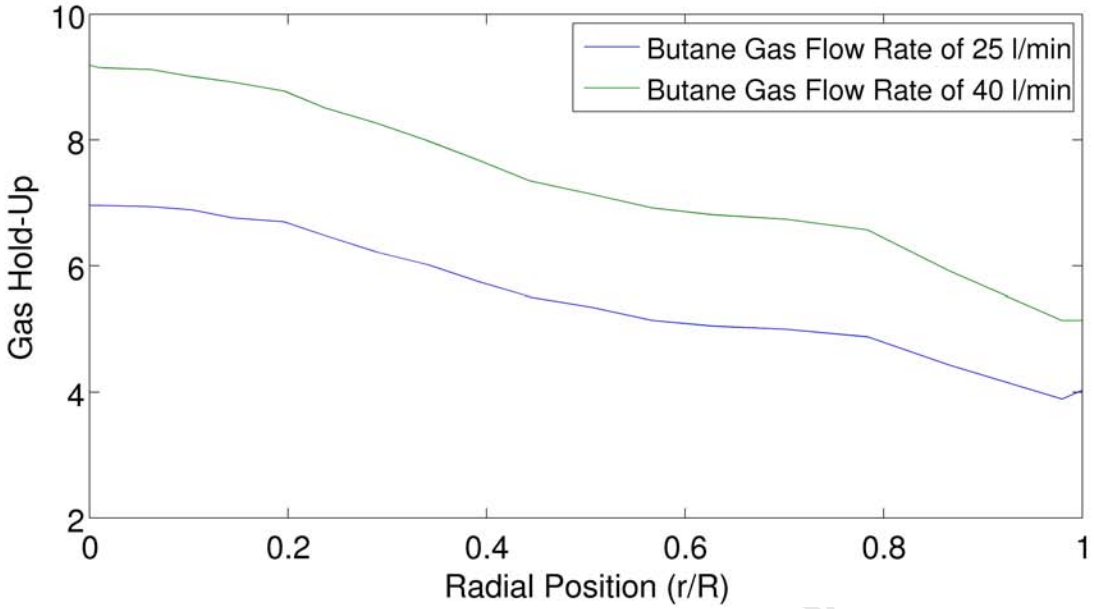

Figure 9.16: Radial gas hold-up profile at an axial distance of 0.83m using the 60^o nozzle